

Calcium Release Mediated by Redox-Sensitive RyR2 Channels Has a Central Role in Hippocampal Structural Plasticity and Spatial Memory

Jamileth Y. More,^{1,*} Barbara A. Bruna,^{1,*} Pedro E. Lobos,¹ José L. Galaz,¹ Paula L. Figueroa,¹ Silvia Namias,¹ Gina L. Sánchez,² Genaro C. Barrientos,² José L. Valdés,^{1,3} Andrea C. Paula-Lima,^{1,4} Cecilia Hidalgo,^{1-3,5} and Tatiana Adasme^{1,6}

Abstract

Aims: Previous studies indicate that hippocampal synaptic plasticity and spatial memory processes entail calcium release from intracellular stores mediated by ryanodine receptor (RyR) channels. In particular, RyR-mediated Ca^{2+} release is central for the dendritic spine remodeling induced by brain-derived neurotrophic factor (BDNF), a neurotrophin that stimulates complex signaling pathways leading to memory-associated protein synthesis and structural plasticity. To examine if upregulation of ryanodine receptor type-2 (RyR2) channels and the spine remodeling induced by BDNF entail reactive oxygen species (ROS) generation, and to test if RyR2 downregulation affects BDNF-induced spine remodeling and spatial memory.

Results: Downregulation of RyR2 expression (short hairpin RNA [shRNA]) in primary hippocampal neurons, or inhibition of nitric oxide synthase (NOS) or NADPH oxidase, prevented agonist-mediated RyR-mediated Ca^{2+} release, whereas BDNF promoted cytoplasmic ROS generation. RyR2 downregulation or inhibitors of N-methyl-D-aspartate (NMDA) receptors, or NOS or of NADPH oxidase type-2 (NOX2) prevented RyR2 upregulation and the spine remodeling induced by BDNF, as did incubation with the antioxidant agent N-acetyl L-cysteine. In addition, intrahippocampal injection of RyR2-directed antisense oligodeoxynucleotides, which caused significant RyR2 downregulation, caused conspicuous defects in a memorized spatial memory task.

Innovation: The present novel results emphasize the key role of redox-sensitive Ca^{2+} release mediated by RyR2 channels for hippocampal structural plasticity and spatial memory.

Conclusion: Based on these combined results, we propose (i) that BDNF-induced RyR2-mediated Ca^{2+} release and ROS generation *via* NOS/NOX2 are strictly required for the dendritic spine remodeling and the RyR2 upregulation induced by BDNF, and (ii) that RyR2 channel expression is crucial for spatial memory processes. *Antioxid. Redox Signal.* 00, 000–000.

Keywords: BDNF, reactive oxygen species, Ca^{2+} signals, dendritic spines, NADPH oxidase, spatial memory training

¹Biomedical Neuroscience Institute, ²Institute of Biomedical Sciences, and ⁴Institute for Research in Dental Sciences, Faculty of Medicine, Universidad de Chile, Santiago, Chile.

³Department of Neuroscience, Faculty of Medicine, Universidad de Chile, Santiago, Chile.

⁵Center for Exercise, Metabolism and Cancer Studies, Faculty of Medicine, Universidad de Chile, Santiago, Chile.

⁶Centro Integrativo de Biología y Química Aplicada, Universidad Bernardo O'Higgins, Santiago, Chile.

*Both these authors share the first authorship.

Innovation

Here, we show that cross talk between ryanodine receptor type-2 (RyR2)-mediated Ca^{2+} release and reactive oxygen species generation is a key feature of the signaling pathways that underlie RyR2 upregulation and the structural remodeling of dendritic spines induced by brain-derived neurotrophic factor (BDNF) in primary hippocampal neurons. We also present results showing that RyR2 channels play a central role in spatial memory processes, since after RyR2 downregulation, rats exhibited strikingly defective performances in a previously memorized spatial memory task. Consequently, the decrease in ryanodine receptor (RyR) levels exhibited by early-stage Alzheimer's disease patients may be a relevant factor for the initial memory defects associated with this neurodegenerative condition.

Introduction

SYNAPTIC CONNECTIONS ARE in continuous remodeling throughout life by way of synapse formation, stabilization, and elimination (23, 24). This remarkable neuronal property makes possible synaptic plasticity, a neuronal attribute characterized by changes in synaptic function and structure. Activity-induced changes in gene expression underlie long-lasting synaptic plasticity, the likely cellular basis of learning and memory (43, 72, 84, 85).

Neurotrophins exert key roles as stringent regulators of synaptic plasticity (91). Earlier studies demonstrated that neurotrophin-induced hippocampal synaptic plasticity exhibits an immediate requirement for protein synthesis (50). Brain-derived neurotrophic factor (BDNF), a neurotrophin that exerts multiple actions, has a central role in the modulation of neuronal activity (18, 73, 107). Increasing hippocampal neuronal activity stimulates the production and release of BDNF (10, 27, 69). High-frequency electrical stimulation of hippocampal cultures promotes BDNF release (38), as does the application of theta-burst trains of action potentials to the same cells (62). BDNF promotes learning and memory tasks and stimulates memory persistence (10, 27, 60, 80, 96).

The central role BDNF plays in synaptic plasticity processes has been described extensively (118). By binding to specific membrane receptors, BDNF promotes changes in the expression of genes involved in synaptic function (75) and plays an important role in neuronal survival and maintenance of several neuronal systems (14). Moreover, by promoting axonal and dendritic growth of neuronal processes, BDNF controls neuronal morphology through the formation and maturation of glutamatergic and GABAergic synapses (19, 36, 44, 91). BDNF mediates pre- and postsynaptic changes related to neuronal activity, which in turn might contribute to sustained synaptic plasticity (22, 45, 64, 65). In addition, BDNF modulates synaptic efficacy by promoting presynaptic transmitter release (5, 105) and by inducing postsynaptic changes that cause long-lasting increases in synaptic plasticity (45, 67).

Neuronal dendritic spines are the primary postsynaptic loci of excitatory synapses and have long been associated with synaptic plasticity (37). Activity-induced release of BDNF from presynaptic neurons prompts the growth of

postsynaptic dendritic spines and the induction and maintenance of long-term potentiation (LTP) in hippocampal area CA1 (10, 11, 27, 110).

BDNF enhances synaptic strength by increasing the open probability of N-methyl-D-aspartate (NMDA) receptor channels *via* BDNF/TrkB-mediated phosphorylation of NMDA receptor subunits (70, 108). This effect depends specifically on the expression of the NMDA receptor NR2B subunit (66, 68). Phosphorylation of the NMDA receptor NR2B subunit, which is particularly critical for synaptic plasticity processes (26, 83, 102), has been linked to BDNF binding to its TrkB membrane receptor during spatial memory formation *via* recruitment of Fyn kinase (79). In the hippocampus, BDNF activates Na^+ inward currents mediated by Nav1.9 (17, 19, 47); the ensuing depolarization promotes Ca^{2+} entry *via* voltage-gated Ca^{2+} channels (61).

Binding of BDNF to TrkB triggers TrkB dimerization, promoting autophosphorylation of tyrosine residues present in the receptor intracellular domains. In turn, TrkB autophosphorylation leads to the recruitment and activation of adapter proteins involved in a range of cellular signaling pathways, including mitogen-activated kinases, phosphatidylinositol 3-kinase, and phospholipase $\text{C}\gamma$ (PLC γ) (16). Hydrolysis of phosphatidylinositol 4,5-bisphosphate by activated PLC γ generates diacylglycerol, a transient activator of protein kinase C, and inositol 1,4,5-trisphosphate (IP $_3$), which through activation of IP $_3$ receptors (IP $_3$ R) triggers Ca^{2+} release from intracellular stores (19).

Calcium release from the endoplasmic reticulum mediated by IP $_3$ R and ryanodine receptor (RyR) channels contributes to the generation of Ca^{2+} signals in response to neuronal activation [reviewed in Baker *et al.* (9), Johenning *et al.* (46), and Paula-Lima *et al.* (93)]. Both channels types, and RyR channels in particular, mediate Ca^{2+} -induced Ca^{2+} release (CICR), a cellular process with a potential role as an amplification mechanism of postsynaptic Ca^{2+} entry signals (13). Immunohistological techniques have revealed heterogeneous IP $_3$ R and RyR expression patterns within neuronal cells of rodent brain (32). Of the three mammalian RyR isoforms, ryanodine receptor type-2 (RyR2) is the most abundant isoform expressed in rat and chicken brain (28, 31).

Earlier work showed that BDNF release induced by high-frequency stimulation of primary hippocampal cultures requires RyR-mediated CICR (10). BDNF also mobilizes Ca^{2+} from intracellular stores *via* IP $_3$ R (19, 40), which through CICR may lead to subsequent Ca^{2+} signal amplification by RyR channels (1, 13, 63, 93). Moreover, BDNF elicits *via* TrkB a nonselective cationic current, which is insensitive to tetrodotoxin and saxitoxin and requires PLC activity and IP $_3$ R activation; this pathway engages intracellular Ca^{2+} stores and extracellular Ca^{2+} entry, suggesting the involvement of TRPC channels in the signaling pathways induced by BDNF (5).

Adding to the complexity of the signaling pathways induced by BDNF, we reported that in primary hippocampal neurons, BDNF engages RyR channels to increase RyR2 and RyR3 protein contents and to induce dendritic spine remodeling (1). These last results agree with previous reports showing that treatment of primary hippocampal neurons with the RyR agonist caffeine promotes RyR-dependent dendritic spine remodeling (58, 59).

Neuronal calcium signals play key roles in memory processes (90). In particular, RyR-mediated calcium release participates

in the acquisition and/or consolidation of spatial memory processes (9, 93). In addition to Ca^{2+} signals, reactive oxygen species (ROS), including superoxide anion, hydrogen peroxide (H_2O_2), and hydroxyl radical, together with reactive nitrogen species (RNS), have important roles in synaptic plasticity processes associated with learning and memory (48, 49, 76, 106). To our knowledge, however, there are no reports showing enhanced ROS generation as part of the complex signaling pathways induced by BDNF in hippocampal neurons.

Here, we report that BDNF promotes ROS generation; this ROS increase is required for BDNF-induced RyR2 upregulation and structural plasticity. Moreover, hippocampal RyR2 downregulation prevented BDNF-induced RyR2 upregulation and dendritic spine remodeling in primary hippocampal neurons, and significantly impaired the performance of rats in a memorized spatial memory task.

Results

Downregulation of the RyR2 isoform significantly inhibits RyR-mediated calcium release

To test the specific involvement of the RyR2 isoform on BDNF-induced synaptic plasticity, we decreased RyR2 expression by transfection of neuron-enriched primary hippocampal cultures (1) with a specific short hairpin RNA (shRNA) against RyR2 (shRyR2).

Immunofluorescence analysis of neuronal cells expressing a red fluorescent protein (RFP) coded in the same vector as the shRyR2 or the shRNA against the scrambled RyR2 sequence ([shScr]; Fig. 1A), indicated that $\sim 30\%$ of the neuronal cells present in the cultures were transfected with shRyR2 or shScr; in addition, RyR2 immunofluorescence in the neuronal soma was 70% lower in shRyR2-RFP-positive neurons (shRyR2, RFP) when compared with shScr-RFP-positive cells (shScr, RFP), or with RFP-negative neurons transfected with shRyR2 (shRyR2) (Fig. 1B), determined by one-way analysis of variance (ANOVA; $F=12.5$; $p<0.0001$), followed by Tukey's *post hoc* test ($***p<0.001$; $n=4$).

Neurons transfected with shScr displayed comparable RyR2 immunofluorescence levels as untransfected controls. Similar results were found at the level of the dendrites (Fig. 1C); statistical analysis was performed by one-way ANOVA ($F=5.0$; $p<0.01$), followed by Tukey's *post hoc* test ($**p<0.01$; $n=4$).

The effects of transfection with shRyR2 or shScr on RyR-mediated Ca^{2+} signals were evaluated in single transfected neurons (RFP positive) loaded with the fluorescent Ca^{2+} -sensitive dye Fluo-4 AM.

As illustrated in a representative experiment, addition of the specific RyR agonist 4-chloro-m-cresol (4-CMC) at a concentration of 0.5 mM generated large fluorescence signals in shScr-transfected neurons, whereas shRyR2-transfected neurons did not respond to the agonist (Fig. 2A).

In contrast, nontransfected neurons present in the same cultures exhibited a significant fluorescence increase of 2.2 ± 0.1 -fold [mean \pm standard error (SE), $n=4$] in response to addition of 0.5 mM 4-CMC. Addition of 4-CMC to neurons transfected with shScr caused a significant increase of maximal Fluo-4 fluorescence, normalized to the average fluorescence value recorded before agonist addition; in contrast, Fluo-4 fluorescence did not increase following 4-CMC addition to shRyR2-transfected neurons (Fig. 2B). The statistical analysis of these results was performed with unpaired

Student's *t*-test ($***p<0.001$; $n=4$). Based on these combined results, we propose that the RyR2 isoform mediates 4-CMC-induced RyR-mediated Ca^{2+} release in primary hippocampal neurons.

Inhibition of nitric oxide synthase or NADPH oxidase type-2 prevents agonist-induced RyR-mediated Ca^{2+} release

Several reports indicate that ROS/RNS stimulate neuronal RyR activity (34, 35, 41, 121). Accordingly, we tested whether pharmacological inhibitors of the nitric oxide synthase (NOS) or NADPH oxidase type-2 (NOX2) enzymes affected agonist-induced RyR-mediated Ca^{2+} release. Primary hippocampal neurons in cultures treated with the NOS inhibitor L-NAME (10 μM) did not display 4-CMC-induced Ca^{2+} release relative to control neurons (Fig. 2C, D). Likewise, treatment with gp91 ds-tat (1.5 μM) to inhibit the NADPH oxidase NOX2 isoform (98) prevented agonist-induced Ca^{2+} release (Fig. 2E, F) compared to neurons treated with the inactive scrambled peptide [Gp91 ds-tat inactive scrambled peptide (gpscr), 1.5 μM]. Statistical analysis of the results presented in Figure 2B, D, and F was performed with unpaired Student's *t*-test ($***p<0.001$; $n=4$).

BDNF-induced ROS generation engages RyR2 channels, NMDA receptors, and NOS and NOX2 activities

To test whether BDNF promotes ROS generation, hippocampal cultures were transfected with the HyPer-Cyto probe to monitor cytoplasmic H_2O_2 production (12). As shown in the representative time-lapse experiment illustrated in Supplementary Figure S1A (Supplementary Data are available online at www.liebertpub.com/ars), addition of BDNF (50 ng/ml) increased probe fluorescence in control neurons, which attained a plateau several minutes after BDNF addition, but not in neurons preincubated with inhibitory ryanodine. Quantification of the maximal fluorescence intensity showed that BDNF significantly increased HyPer-Cyto fluorescence levels (1.74 ± 0.08) over the basal value, indicated by a segmented line in Figure 3A; of note, cultures preincubated with inhibitory ryanodine (50 μM), which was maintained during the experiment, exhibited lower fluorescence levels (0.41 ± 0.1) than control cells (Fig. 3A).

Representative time-lapse experiments (Supplementary Fig. S1B) show that addition of BDNF (50 ng/ml) significantly increased HyPer-Cyto fluorescence in neurons transfected with shScr, whereas it caused similar reductions of fluorescence intensity in neurons transfected with shRyR2 or treated with inhibitory ryanodine. The average results illustrated in Figure 3B show that BDNF addition (50 ng/ml) significantly increased probe fluorescence (1.59 ± 0.02) in neuronal cells transfected with the shScr sequence; in contrast, neurons transfected with shRyR2 displayed a lower level of fluorescence (0.55 ± 0.11) than that exhibited by neurons transfected with shScr or by control neurons. Statistical analysis of the results presented in Figure 3A and B was performed with unpaired Student's *t*-test ($***p<0.001$; $n=5$).

Next, we tested whether MK801, a synaptic NMDA receptor inhibitor, affected BDNF-induced ROS generation. A representative time-lapse experiment (Supplementary Fig. S1C) shows that control cells transfected with the

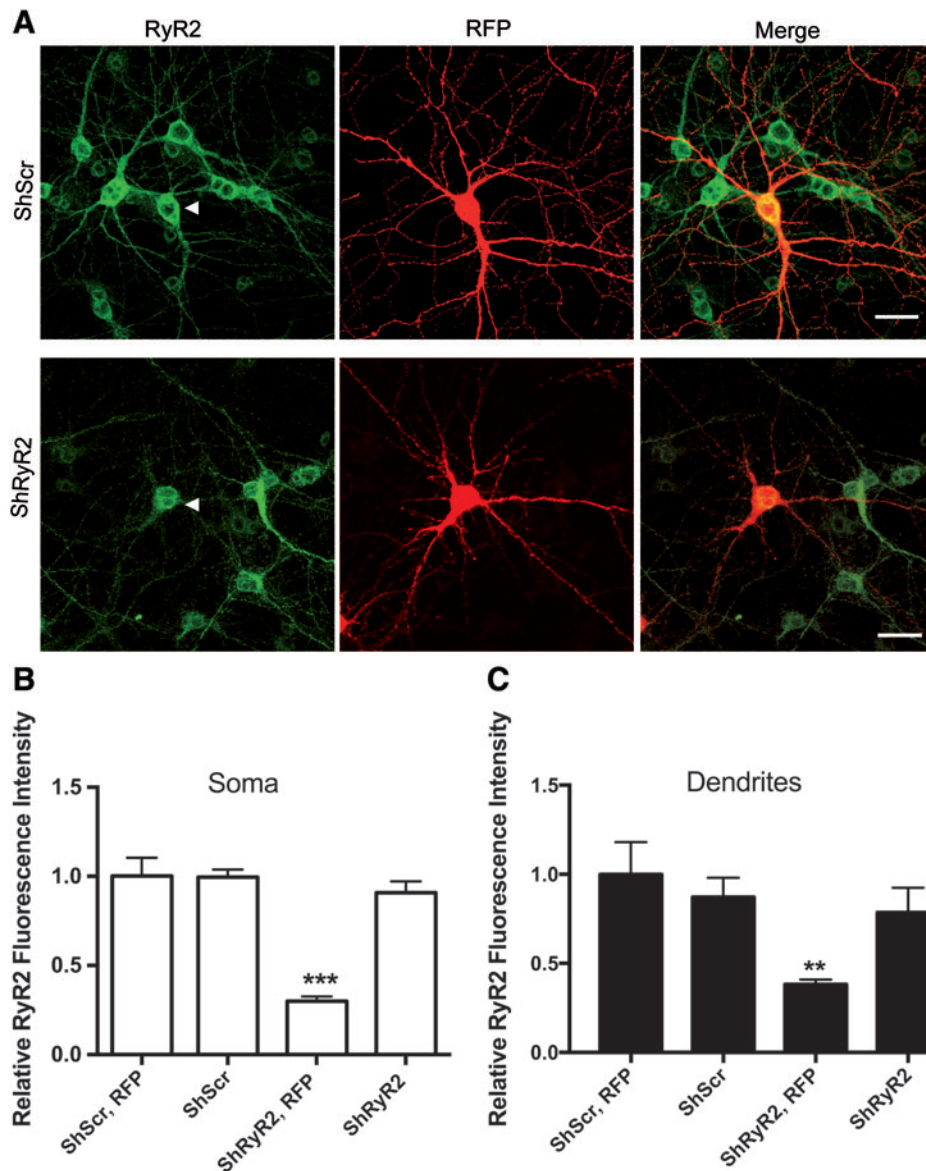


FIG. 1. Effects of shRyR2 transfection over RyR2 levels in single hippocampal neurons. (A) Representative immunofluorescence images collected 48 h after transfection with the shRyR2 or shScr vectors coupled to the RFP sequence. *Green*: RyR2 immunodetection; *red*: neurons expressing shRyR2 or shScr coupled to RFP. The *arrowheads* shown in the *left panels* indicate the transfected neuronal cells. Scale bar = 20 μ m. Quantification of RyR2 green fluorescence intensity in the soma (B) or dendrites (C) of neurons expressing the shRyR2 or shScr, and in untransfected neurons. Values represent mean \pm SE ($n=4$). Statistical analysis of the results presented in (B) was performed with one-way ANOVA ($F=12.5$; $p<0.0001$), followed by Tukey's *post hoc* test ($***p<0.001$). Statistical analysis of the results presented in (C) was performed with one-way ANOVA ($F=5.0$; $p<0.01$), followed by Tukey's *post hoc* test ($**p<0.01$). ANOVA, analysis of variance; RFP, red fluorescent protein; RyR2, ryanodine receptor type-2; SE, standard error; shRNA, short hairpin RNA; shRyR2, shRNA against RyR2; shScr, shRNA against the scrambled RyR2 sequence. To see this illustration in color, the reader is referred to the web version of this article at www.liebertpub.com/ars

HyPer-Cyto probe displayed increased fluorescence following BDNF addition (50 ng/ml); in contrast, neuronal cells preincubated with MK801 (10 μ M, 30 min) displayed a significant fluorescence decrease following BDNF addition. Quantification of results shows that while control neurons displayed a significant increase in HyPer-Cyto fluorescence following BDNF addition, neurons preincubated with MK-801 displayed a significant reduction (Fig. 3C). Statistical analysis of the results presented in Figure 3C was performed with unpaired Student's *t*-test ($***p<0.001$; $n=5$).

Previous studies in primary cortical neurons have shown that stimulation of NMDA receptors promotes ROS generation *via* sequential stimulation of the NOS and NOX2 enzymes (31). Accordingly, we tested next whether NOS or NOX2 inhibitors affected BDNF-induced ROS generation. To this aim, we preincubated primary cultures transfected with the HyPer-Cyto probe for 30 min with L-NAME (10 μ M), a universal inhibitor of all NOS isoforms. A representative experiment (Supplementary Fig. S1D) shows that addition of BDNF (50 ng/ml) to cultures incubated with L-

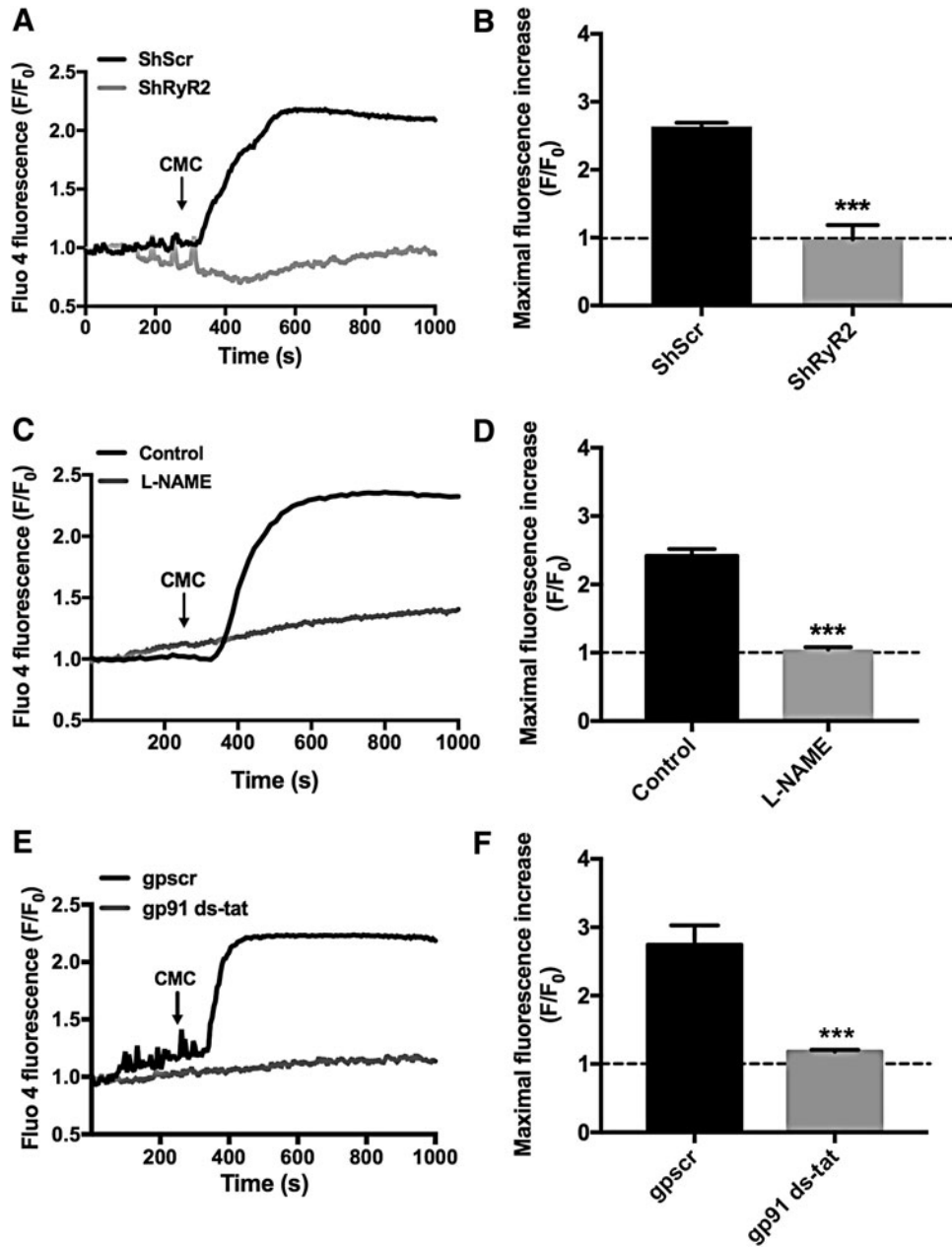


FIG. 2. RyR-mediated Ca^{2+} release induced by the agonist 4-CMC. Determination of fluorescence signals elicited by the RyR agonist 4-CMC in primary hippocampal cultures loaded with the Ca^{2+} -sensing probe Fluo-4. Fluorescence signals are expressed as F/F_0 , where F_0 represents the basal fluorescence recorded from several ROIs in the soma before addition of 0.5 mM 4-CMC. (A) Representative time-lapse experiment showing Fluo-4 fluorescence recorded in the soma of neurons transfected for 48 h with the shRyR2 (gray trace) or shScr (black trace) vectors coupled to the RFP sequence; addition of 4-CMC is indicated by an arrow. Transfected neurons were identified by the red color provided by the coupled RFP vector. (B) Quantification of the results illustrated in (A). (C) Representative time-lapse experiment showing average Fluo-4 fluorescence recorded from several ROIs in the soma of neurons from cultures incubated with the NOS inhibitor L-NAME (10 μM , gray trace) and from neurons present in control cultures (black trace). (D) Quantification of the results illustrated in (C). (E) Representative time-lapse experiment showing average Fluo-4 fluorescence recorded from several ROIs in the soma of neurons from cultures preincubated for 30 min with the NOX2 inhibitor peptide gp91 ds-tat (1.5 μM , gray trace) or the control peptide gpscr (1.5 μM , black trace). (F) Quantification of the results illustrated in (E). (B, D, F) Values correspond to mean \pm SE ($n=4$). Statistical analysis of the results presented in (B, D, F) was performed with unpaired Student's t -test (***) $p < 0.001$. 4-CMC, 4-chloro-m-cresol; gpscr, Gp91 ds-tat inactive scrambled peptide; NOS, nitric oxide synthase; NOX2, NADPH oxidase type-2; ROI, region of optical interest; RyR, ryanodine receptor.

NAME led to a gradual decrease of probe fluorescence with time; in comparison, control neurons displayed increased HyPer-Cyto fluorescence levels following BDNF addition. To test if NOX2 inhibition affected BDNF-induced ROS generation, we treated cultures with the NOX2 inhibitor gp91 ds-tat or with the control probe gpcr. BDNF addition (50 ng/ml) to cultures transfected with the HyPer-Cyto probe and preincubated for 30 min with gp91 ds-tat (1.5 μ M) induced a decrease in probe fluorescence with time; in contrast, BDNF addition (50 ng/ml) to cultures preincubated for 30 min with gpcr (1.5 μ M) caused a significant increase in probe fluorescence (Supplementary Fig. S1E). Quantification of these results shows that pharmacological inhibition of the NOS (Fig. 3D) or the NOX2 (Fig. 3E) enzymes suppressed BDNF-induced H₂O₂ generation. Statistical analysis of the results presented in Figure 3D and E was performed with unpaired Student's *t*-test (***p* < 0.001; *n* = 5).

A previous report in neocortical neuronal cultures described that NMDA receptor activation induces a sequential signaling cascade entailing calcium-dependent NOS activation, nitric oxide generation, increased cyclic GMP production, activation of protein kinase G (PKG), and NOX2 activation (33). A subsequent report described BDNF-induced NOS activation in primary hippocampal neurons (57). Accordingly, we tested the effects of the PKG inhibitor KT-5823 (116) on BDNF-induced ROS generation. As illustrated in Figure 3F and Supplementary Figure S1F, addition of BDNF (50 ng/ml) suppressed BDNF-induced ROS generation, showing that PKG activity mediates the ROS increase induced by BDNF. Statistical analysis of the results presented in Figure 3F was performed with unpaired Student's *t*-test (***p* < 0.001; *n* = 3).

Based on these combined results, we propose that BDNF-induced cytoplasmic H₂O₂ generation requires sequential NOS and NOX2 activation in response to BDNF-induced NMDA receptor stimulation, plus Ca²⁺ signals initially produced by Ca²⁺ influx *via* NMDA receptors and subsequently amplified through RyR2-mediated CICR.

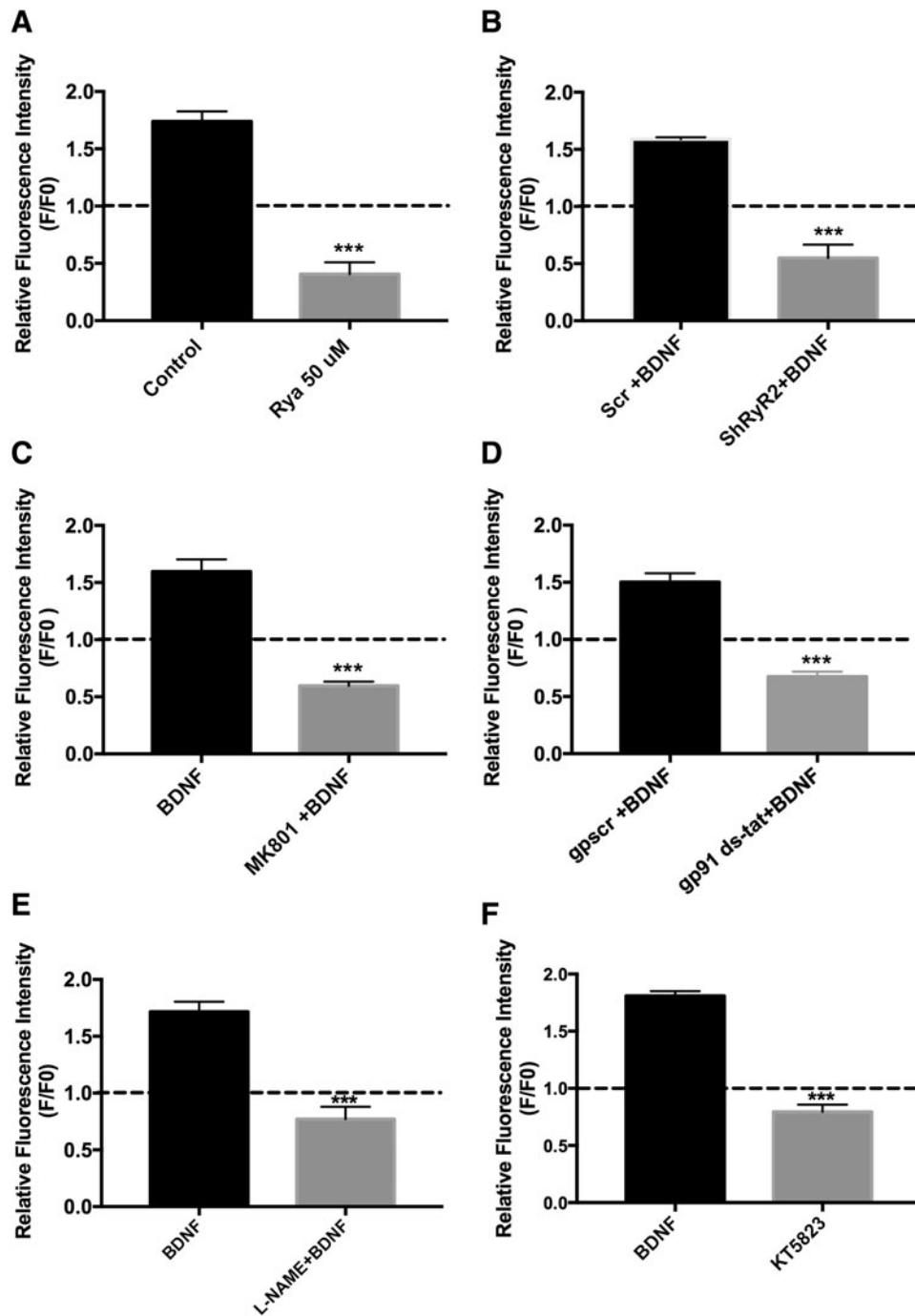
BDNF-induced RyR2 upregulation entails RyR2-mediated Ca²⁺ release plus ERK1/2, NOS, and NOX activities

RyR2-mediated Ca²⁺ release. Previously, we reported that BDNF-induced RyR2 upregulation requires functional RyR channels (1).

To test the specific contribution of the RyR2 isoform to BDNF-induced RyR2 upregulation, primary hippocampal neurons were transfected with shRyR2 or shScr and subsequently exposed to BDNF. Transfected cultures displayed a percent reduction of RyR2 messenger RNA (mRNA) levels of 54 ± 7 (*n* = 5) and a percent reduction of protein content of 38 ± 8 (*n* = 8) relative to cultures transfected with shScr, as illustrated in Figure 4A and B, respectively. Following incubation with BDNF (50 ng/ml) for 6 h, primary cultures transfected with shScr displayed a significant increase (1.8-fold) in RyR2 mRNA (Fig. 4A), determined by one-way ANOVA (*F* = 48.0; *p* < 0.0001), followed by Tukey's *post hoc* test (***p* < 0.001; *n* = 5). Likewise, RyR2 protein levels increased significantly following BDNF addition (50 ng/ml), (Fig. 4B), determined by one-way ANOVA (*F* = 6.6; *p* < 0.005), followed by Tukey's *post hoc* test (**p* < 0.05; ***p* < 0.01; *n* = 8). Cultures transfected with shRyR2 displayed lower RyR2 mRNA and protein levels than cultures transfected with shScr; BDNF addition (50 ng/ml) increased RyR2 mRNA and protein in these cultures only to the levels exhibited by shScr-transfected cultures not treated with BDNF (Fig. 4A, B; see also original immunoblots in Supplementary Fig. S7A). These modest increments presumably reflect the response to BDNF of untransfected neurons present in the culture.

The primary hippocampal cultures used in this work displayed significant RyR2 and RyR3 mRNA levels, with average cycle threshold (Ct) values for RyR2 and RyR3 of 24 and 26, respectively. In contrast, the average Ct value for RyR1 was 35, beyond the quantitative polymerase chain reaction (qPCR) detection range; this value did not reflect the use of an inadequate primer, because this primer yielded an average Ct value of 20 for RyR1 in rat skeletal muscle

FIG. 3. BDNF induces ROS generation in primary hippocampal neurons. Primary hippocampal cultures were transfected with the HyPer-Cyto sensor to detect changes in cytoplasmic H₂O₂ levels. Probe fluorescence was measured by confocal microscopy. Fluorescence signals are expressed as *F*/*F*₀, where *F*₀ represents the basal fluorescence recorded from several ROIs in the soma before addition of BDNF (50 ng/ml); values measured 2800 s after BDNF addition were quantified. (A) Quantification of relative HyPer-Cyto fluorescence recorded after BDNF addition (50 ng/ml) in the soma of neurons from control cultures (black bar) or from cultures preincubated for 60 min with 50 μ M ryanodine to abolish RyR activity (gray bar). (B) Quantification of relative HyPer-Cyto fluorescence after BDNF addition (50 ng/ml) in the soma of neurons from cultures transfected with the vectors shScr (black bar) or shRyR2 (gray bar) coupled to the RFP sequence. Transfected neurons were identified by the red color provided by the coupled RFP vector. (C) Quantification of relative HyPer-Cyto fluorescence measured after BDNF addition (50 ng/ml) in the soma of neurons from control cultures (black bar) or from cultures preincubated for 30 min with the NMDA receptor inhibitor MK801 (10 μ M, gray bar); this inhibitor was kept during the subsequent incubation with BDNF. (D) Quantification of relative HyPer-Cyto fluorescence measured after BDNF addition (50 ng/ml) in the soma of neurons from control cultures (black bar) or from cultures preincubated for 30 min with the NOS inhibitor L-NAME (10 μ M, gray bar); L-NAME was kept during the subsequent incubation with BDNF. (E) Quantification of relative HyPer-Cyto fluorescence measured after BDNF addition (50 ng/ml) in the soma of neurons preincubated for 30 min with the control gpcr peptide (1.5 μ M, black bar) or with the NOX2 inhibitor gp91 ds-tat peptide (1.5 μ M, gray bar). (F) Quantification of relative HyPer-Cyto fluorescence measured after BDNF addition (50 ng/ml) in the soma of neurons from control cultures (black bar) or from cultures preincubated for 15 min with the PKG inhibitor KT-5823 (5 μ M, gray bar); this inhibitor was kept during the subsequent incubation with BDNF. Results are expressed as mean ± SE [*n* = 5, except for (F), where *n* = 3]. Statistical analysis of these results was performed with unpaired Student's *t*-test (***p* < 0.001). BDNF, brain-derived neurotrophic factor; H₂O₂, hydrogen peroxide; NMDA, N-methyl-D-aspartate; PKG, protein kinase G; ROS, reactive oxygen species; Rya, ryanodine.



homogenates. Likewise, the primary hippocampal cultures used in this work exhibited negligible RyR1 protein levels in immunoblots performed with a highly specific RyR1 antibody (manuscript in preparation).

Cultures transfected with shRyR2 showed similar RyR3 mRNA levels as cultures transfected with shScr; incubation for 6 h with BDNF (50 ng/ml) produced similar increases in RyR3 mRNA levels in Src-transfected (2.2-fold) as in shRyR2-transfected (2.0-fold) cultures (Supplementary Fig. S2A), showing that transfection with shRyR2 did not affect basal RyR3 mRNA levels or the increase in these levels produced by BDNF. In addition, transfection with shRyR2 did not modify basal RyR3 protein content and did not prevent the RyR3 protein increase induced by BDNF (Supplementary Fig. S2B).

Based on these combined results, which confirm the specificity of the shRyR2 sequence used here, and on previous reports showing that the RyR2 isoform predominates in the hippocampus (31), we propose that RyR2-mediated Ca^{2+} release plays a prominent role in the RyR2 upregulation induced by BDNF.

ERK1/2. To prevent downstream ERK1/2 activation in response to BDNF (4), we used U0126 to inhibit the mitogen-activated protein kinase MEK. Cultures preincubated for 30 min with U0126 (10 μ M), which was maintained during the subsequent incubation with BDNF (50 ng/ml), did not exhibit increased RyR2 mRNA and protein levels following incubation with BDNF for 6 h; in contrast, a significant increase in RyR2 mRNA and protein content occurred in control neurons treated

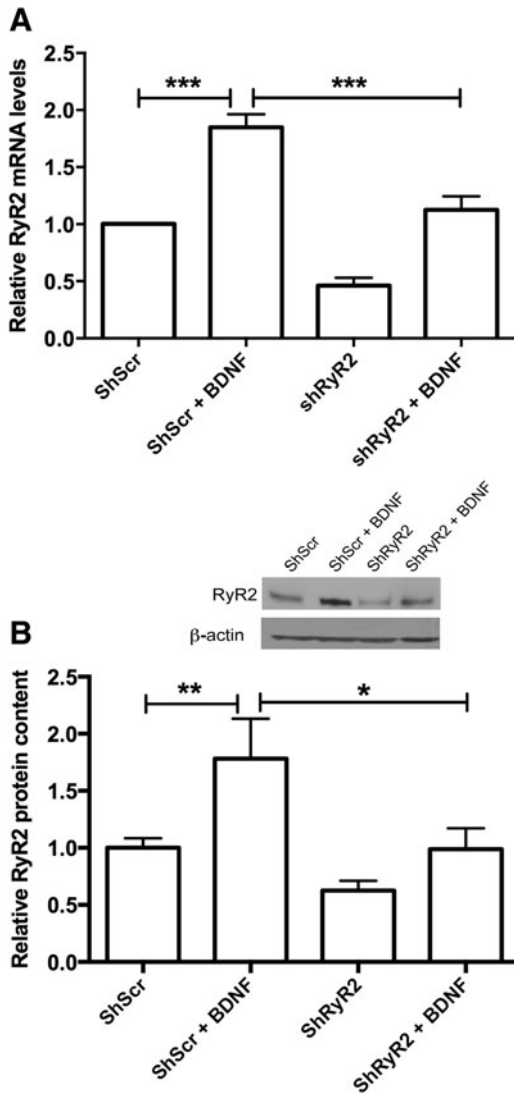


FIG. 4. Effects of BDNF and RyR2 downregulation on RyR2 mRNA and protein levels. Hippocampal neurons were transfected with shRyR2 or shScr; 48 h after transfection, cultures were incubated for 6 h with BDNF (50 ng/ml). Total mRNA and protein content was determined by qPCR and Western blot analysis, respectively; values are expressed relative to β -actin levels. **(A)** Quantification of RyR2 mRNA levels. **(B)** Quantification of RyR2 protein content. A representative blot is shown above the graph. Results are expressed as mean \pm SE. Statistical analysis of the results presented in **(A)** ($n=5$) was performed with one-way ANOVA ($F=48.0$; $p<0.0001$), followed by Tukey's *post hoc* test ($***p<0.001$). Statistical analysis of the results presented in **(B)** ($n=8$) was performed with one-way ANOVA ($F=6.6$; $p<0.005$), followed by Tukey's *post hoc* test ($*p<0.05$; $**p<0.01$). mRNA, messenger RNA; qPCR, quantitative polymerase chain reaction.

with BDNF (Fig. 5A, B; see also original immunoblot in Supplementary Fig. S7B). Statistical analysis of these results was performed with one-way ANOVA ($F=11.5$; $p=0.0002$ for Fig. 5A; $F=8.7$; $p=0.0003$ for Fig. 5B), followed by Tukey's *post hoc* test ($**p<0.01$; $***p<0.001$; $n=5$).

Reactive oxygen species. To elucidate whether BDNF-induced H_2O_2 generation contributed to BDNF-induced

RyR2 upregulation, cultures were preincubated for 30 min with the universal ROS scavenger N-acetylcysteine (NAC, 10 mM), which was kept during the subsequent 6-h incubation period with BDNF (50 ng/ml). Control cultures incubated with BDNF displayed increased levels of both RyR2 mRNA and protein, with values five- and twofold higher, respectively, over the controls, while NAC treatment prevented these increments (Fig. 5C, D; see also original immunoblot in Supplementary Fig. S7C). Statistical analysis of these results was performed with one-way ANOVA ($F=16.3$; $p<0.0001$ for Fig. 5C; $F=10.0$; $p=0.0007$ for Fig. 5D), followed by Tukey's *post hoc* test ($*p<0.05$; $***p<0.001$; $n=5$).

NOS and NOX2. Cultures preincubated for 30 min with L-NAME (10 μ M) and subsequently incubated with BDNF (50 ng/ml, 6 h) in the presence of L-NAME did not display significant increases in RyR2 mRNA and protein levels exhibited by control cultures following BDNF addition (50 ng/ml) (Fig. 5E, F; see also original immunoblot in Supplementary Fig. S7D). Statistical analysis of these results was performed with one-way ANOVA ($F=11.2$; $p=0.0002$ for Fig. 5E; $F=7.7$; $p=0.004$ for Fig. 5F), followed by Tukey's *post hoc* test ($*p<0.05$; $**p<0.01$; $***p<0.001$; $n=5$). Likewise, incubation with BDNF (50 ng/ml, 6 h) of cultures treated with the gp91 ds-tat inhibitory peptide (1.5 μ M, preincubated 30 min, kept for 6 h of incubation with BDNF) did not lead to RyR2 upregulation, which did occur in cultures treated with the scrambled peptide gpcr (1.5 μ M, preincubated 30 min, kept for 6 h of incubation with BDNF) (Fig. 5G; see also original immunoblot in Supplementary Fig. S7E). Statistical analysis of the results presented in Figure 5G was performed with one-way ANOVA ($F=7.4$; $p=0.0005$), followed by Tukey's *post hoc* test ($**p<0.01$; $n=5$).

Based on these combined results, we suggest that BDNF-induced RyR2 upregulation entails a complex set of Ca^{2+} -dependent signaling cascades, including RyR2-mediated Ca^{2+} release and ERK1/2, NOS, and NOX2 activation, leading to H_2O_2 generation.

RyR2-mediated Ca^{2+} release, ROS, NOS, and NOX2 mediate BDNF-induced dendritic spine remodeling

Changes in dendritic spine morphology induced by caffeine (58) or BDNF (1) require functional RyR channels. Here, we investigated if RyR2 downregulation affected the short-term and long-term changes in spine morphology induced by BDNF or caffeine. Addition of BDNF (50 ng/ml) to neurons transfected with shScr (detected by their green fluorescence) promoted spine elongation, as illustrated by a representative experiment (Fig. 6A). These changes, which on average took place as early as 15 min after BDNF addition (Fig. 6B), did not occur in neurons transfected with shRyR2, identified by their green fluorescence (Fig. 6A, B). Statistical analysis of the results presented in Figure 6B was performed with two-way ANOVA [interaction: $F_{(8,87)}=4.5$; $p=0.0001$; row factor: $F_{(4,87)}=0.7$; $p=0.57$; column factor: $F_{(2,87)}=49.8$; $p=0.0001$], followed by Bonferroni's *post hoc* test ($n=5$). The corresponding p -values are given in Figure 6B legend.

To test if BDNF-induced ROS generation was required for BDNF-induced spine remodeling, we preincubated cultures for 30 min with 10 mM NAC. This treatment produced a

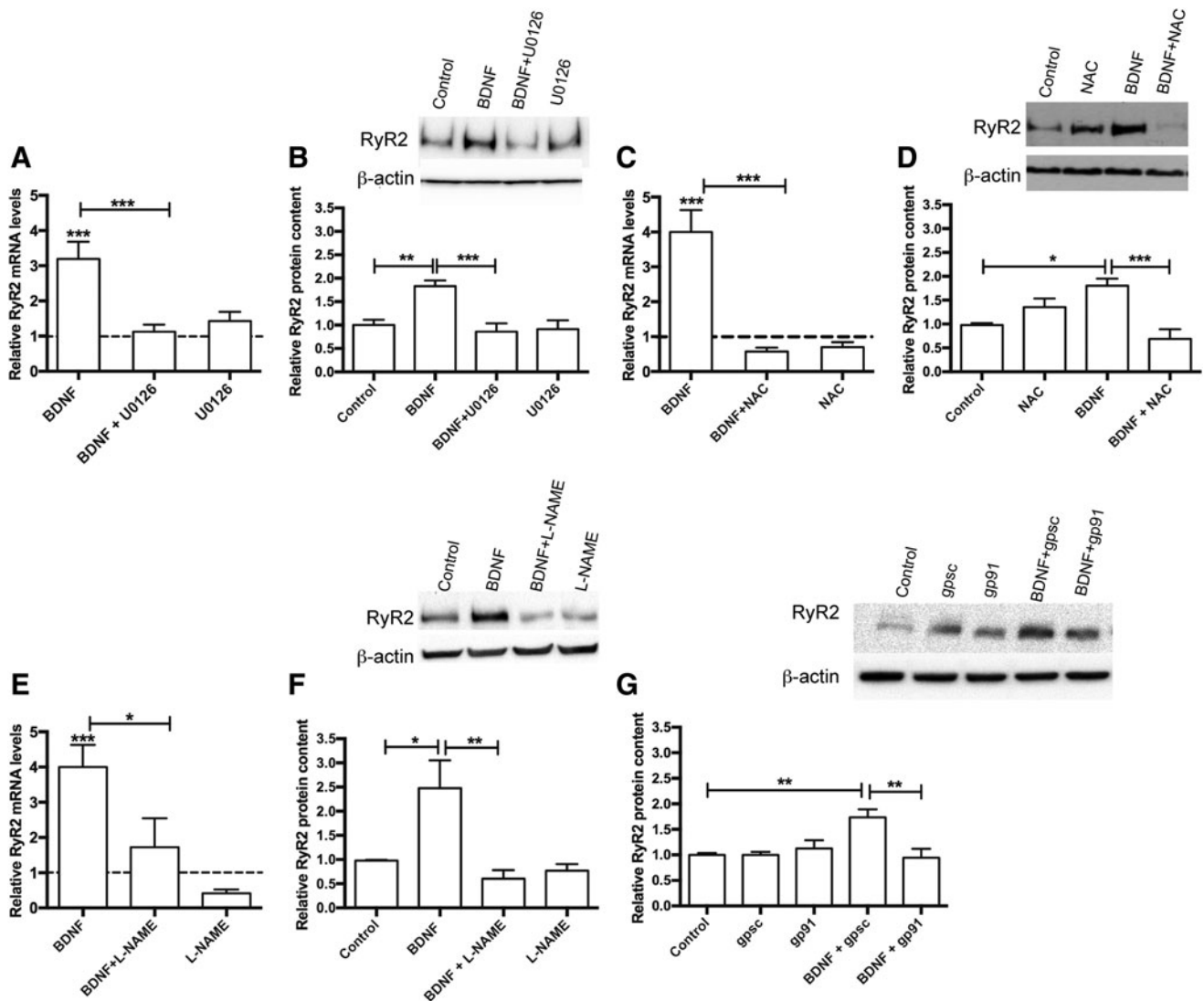


FIG. 5. BDNF-induced RyR2 upregulation requires ERK1/2, NOS, and NOX2 activities and is prevented by NAC. Primary hippocampal neurons were preincubated for 30 min with inhibitors of ERK1/2, NOS, or NOX2 or with NAC; inhibitors and NAC were maintained during the 6 h of incubation with BDNF (50 ng/ml). RyR2 mRNA levels were normalized with respect to the relative levels of β -actin. RyR2 protein content was determined by Western blot analysis; RyR2 protein band densities were quantified and normalized relative to β -actin protein levels. (A) Relative RyR2 mRNA levels and (B) relative RyR2 protein content in cultures treated with BDNF plus/minus the ERK1/2 inhibitor U0126 (10 μ M). Statistical analysis of these results was performed with one-way ANOVA [$F=11.5$; $p=0.0002$ for (A); $F=8.7$; $p=0.0003$ for (B)], followed by Tukey's *post hoc* test (** $p<0.01$; *** $p<0.001$). (C) Relative RyR2 mRNA levels and (D) relative RyR2 protein content in cultures treated with BDNF \pm 10 mM NAC. Statistical analysis of these results was performed with one-way ANOVA [$F=16.3$; $p<0.0001$ for (C); $F=10.0$; $p=0.0007$ for (D)], followed by Tukey's *post hoc* test (* $p<0.05$; *** $p<0.001$). (E) Relative RyR2 mRNA levels and (F) relative RyR2 protein content of cultures treated with BDNF plus/minus the NOS inhibitor L-NAME (10 μ M). Statistical analysis of these results was performed with one-way ANOVA [$F=11.2$; $p=0.0002$ for (E); $F=7.7$; $p=0.004$ for (F)], followed by Tukey's *post hoc* test (* $p<0.05$; ** $p<0.01$; *** $p<0.001$). (G) Relative RyR2 protein content of cultures treated with BDNF plus the NOX2 inhibitor peptide gp91 (1.5 μ M) or its inactive analog gp91 (1.5 μ M). Statistical analysis of the results presented in (G) was performed with one-way ANOVA ($F=7.4$; $p=0.0005$), followed by Tukey's *post hoc* test (** $p<0.01$). Results represent mean \pm SE ($n=5$). NAC, N-acetylcysteine.

significant reduction in the spine lengthening induced by BDNF (50 ng/ml) (Fig. 6C, D). Statistical analysis of the results presented in Figure 6D was performed with two-way ANOVA [interaction: $F_{(8,105)}=7.4$; $p=0.0001$; row factor: $F_{(4,105)}=18.0$; $p=0.0001$; column factor: $F_{(2,105)}=88.9$; $p=0.0001$], followed by Dunnett's *post hoc* test ($n=8$). The corresponding p -values are given in Figure 6D legend.

Addition of 10 mM caffeine to transfected cultures promoted, after 15 min (the first time point tested), significant spine elongation in neurons transfected with shScr but not in neurons transfected with shRyR2 (Fig. 6E, F). Statistical analysis of the results presented in Figure 6F was performed with two-way ANOVA [interaction: $F_{(8,93)}=2.6$; $p<0.01$; row factor: $F_{(4,93)}=1.7$; $p=0.15$; column factor: $F_{(2,93)}=40.6$;

$p=0.0001$], followed by Dunnett's *post hoc* test ($n=8$). The corresponding p -values are given in Figure 6F legend. Of note, the effects of caffeine, which stimulates RyR activity directly, were faster than the BDNF-elicited changes. Presumably, BDNF stimulates RyR2-mediated Ca^{2+} release by engaging first other upstream signaling cascades.

In addition, NAC largely prevented the spine lengthening induced by caffeine (Fig. 6G, H). In fact, neurons treated with NAC (10 mM) exhibited on average a net decrease in spine length even after addition of 10 mM caffeine (Fig. 6H). Statistical analysis of the results presented in Figure 6H was performed with two-way ANOVA [interaction: $F_{(12,165)}=5.1$; $p=0.0001$; row factor: $F_{(4,165)}=2.3$; $p=0.06$; column factor: $F_{(3,165)}=71.7$; $p=0.0001$], followed by Dunnett's *post hoc* test ($n=8$). The corresponding p -values are given in Figure 6H legend.

Next, we evaluated at long term, spine morphology changes in neurons present in cultures incubated for 6 h with BDNF (50 ng/ml). As illustrated in Figure 7A and B, BDNF produced a marked increase in spine density in neurons transfected with shScr but not in neurons transfected with shRyR2. Statistical analysis of the results presented in Figure 7B was performed with one-way ANOVA ($F=23.0$; $p=0.0001$), followed by Tukey's *post hoc* test ($***p<0.001$; $n=5$).

Similarly, incubation with caffeine (10 mM, 6 h) caused a substantial increase in spine density in neurons transfected with shScr, whereas shRyR2-transfected neurons did not undergo caffeine-induced spine remodeling (Fig. 7C, D). Statistical analysis of the results presented in Figure 7D was performed with one-way ANOVA ($F=6.8$; $p=0.002$), followed by Tukey's *post hoc* test ($*p<0.05$; $**p<0.01$; $n=5$).

To examine whether the long-term structural plasticity changes induced by BDNF in hippocampal neurons required ROS, we preincubated the cultures for 30 min with NAC (10 mM) before BDNF addition. NAC-treated neurons displayed a significant decrease in dendritic spine density relative to controls and did not present the density increase displayed by control neurons incubated for 6 h with BDNF

(50 ng/ml), (Fig. 8A, B). Statistical analysis of the results presented in Figure 8B was performed with one-way ANOVA ($F=38.1$; $p=0.0001$), followed by Tukey's *post hoc* test ($***p<0.001$; $n=5$).

We studied next the possible participation of NOS and NOX2 as sources of ROS generation on BDNF-induced spine remodeling. Cultures preincubated for 30 min with 10 μM L-NAME, which was maintained during the 6 h of incubation with BDNF (50 ng/ml), did not present an increase in spine density (Fig. 8C, D). Statistical analysis of the results presented in Figure 8D was performed with one-way ANOVA ($F=45.1$; $p=0.0001$), followed by Tukey's *post hoc* test ($***p<0.001$; $n=5$). Likewise, the NOX2 inhibitor gp91 ds-tat (1.5 μM) prevented spine density increase produced by 6 h of incubation with BDNF, while neurons treated with the gpcr peptide (1.5 μM) displayed significantly increased spine density (Fig. 8E, F). Statistical analysis of the results presented in Figure 8F was performed with one-way ANOVA ($F=7.2$; $p=0.015$), followed by Tukey's *post hoc* test ($*p<0.05$; $n=4$).

We infer from these combined results that ROS generated by sequential activation of the NOS and NOX2 enzymes, together with RyR2-mediated Ca^{2+} release, play key roles as signaling molecules in the short- and long-term spine remodeling induced by BDNF or caffeine.

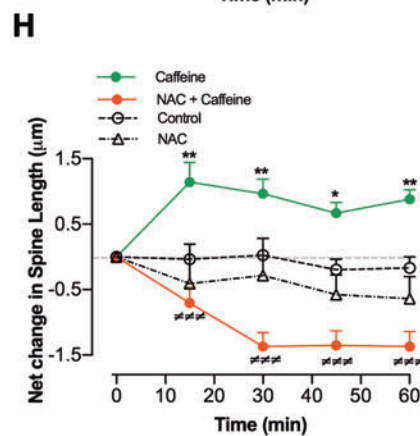
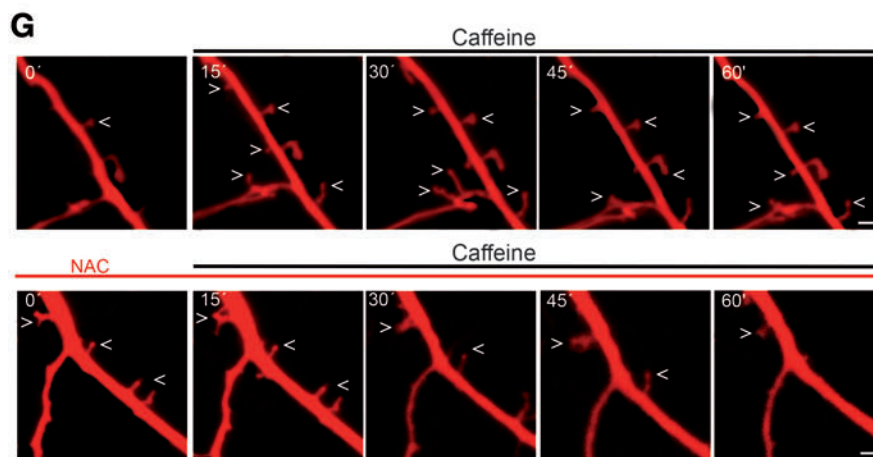
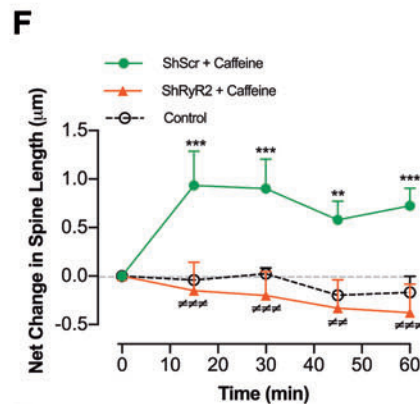
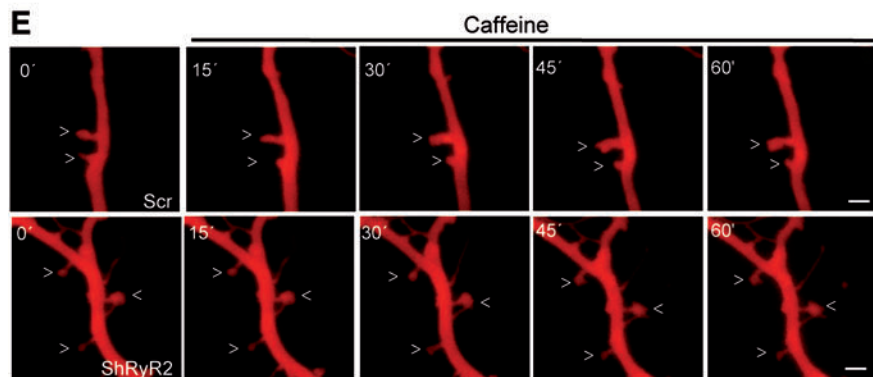
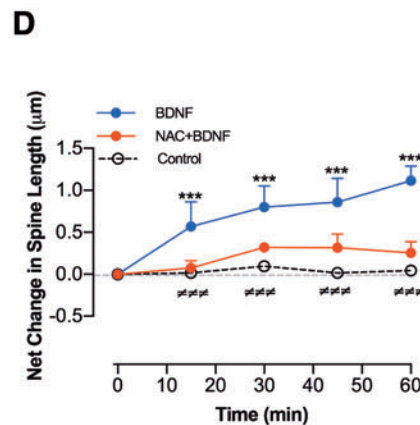
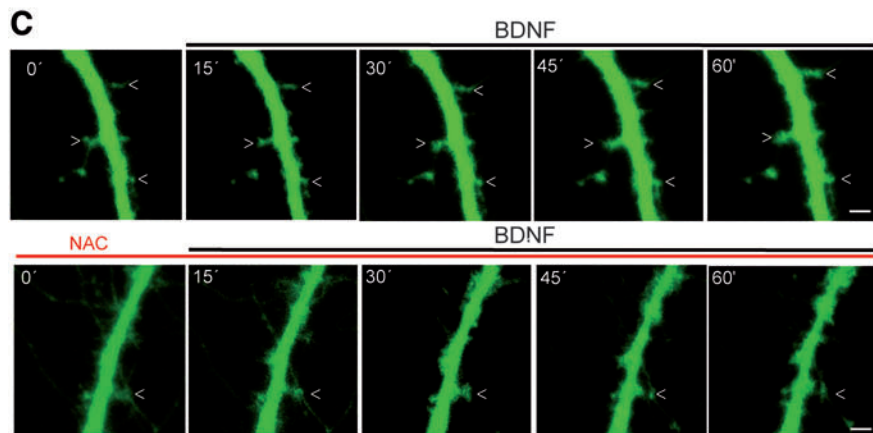
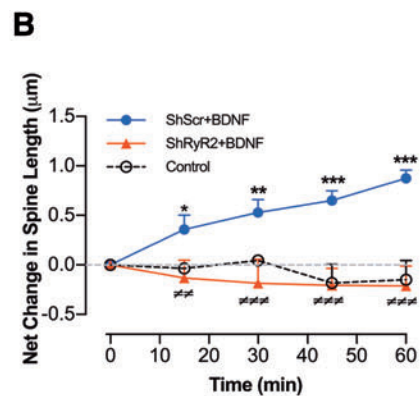
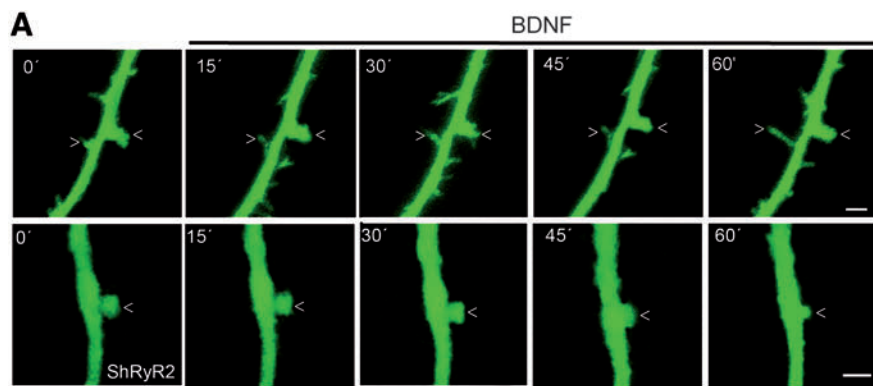
Downregulation of the RyR2 isoform causes significant defects in a memorized spatial memory task

To test if RyR2 downregulation affected spatial memory processes, we placed cannulas in the CA1 region. To evaluate hippocampal-dependent spatial learning and memory, cannulated animals (male rats) were trained during 9 consecutive sessions in the Oasis maze task, which represents a dry version of the Morris water maze (25, 53) and involves searching for the reward (water) in one of 21 equidistant wells on a circular arena provided with visual cues (Supplementary Fig. S3).

After the third training session, we performed bilateral injections of animals three times in a period of 25 h (see Table

FIG. 6. RyR2 downregulation or NAC inhibit the dendritic spine elongation induced by BDNF or caffeine.

(A) Representative images of dendrites from neurons transfected with shScr (top panels) or shRyR2 (lower panels) plus GFP. (B) Quantification of spine length changes with time measured in control neurons and in neurons transfected with shRyR2 or shScr following BDNF addition. Values represent mean \pm SE ($n=5$). Statistical analysis was performed with two-way ANOVA [interaction: $F_{(8,87)}=4.5$; $p=0.0001$; row factor: $F_{(4,87)}=0.7$; $p=0.57$; column factor: $F_{(2,87)}=49.8$; $p=0.0001$], followed by Bonferroni's *post hoc* test. $**p<0.01$ and $***p<0.001$ shScr plus BDNF versus shScr; $***p<0.001$ shScr plus BDNF versus shRyR2 plus BDNF. (C) Representative images of dendrites expressing GFP preincubated for 30 min with 10 mM NAC and treated with BDNF. (D) Quantification of spine length changes with time determined in control neurons or in neurons preincubated with 10 mM NAC. Values represent mean \pm SE ($n=8$). Statistical analysis was performed with two-way ANOVA [interaction: $F_{(8,105)}=7.4$; $p=0.0001$; row factor: $F_{(4,105)}=18.0$; $p=0.0001$; column factor: $F_{(2,105)}=88.9$; $p=0.0001$], followed by Dunnett's *post hoc* test. $***p<0.001$ BDNF versus control; $***p<0.001$ BDNF versus BDNF+NAC. (E) Representative images of dendrites from neurons expressing shRyR2 or shScr+RFP incubated with 10 mM caffeine. (F) Quantification of spine length changes with time determined in control neurons or in neurons transfected with shRyR2 or shScr following caffeine addition. Values represent mean \pm SE ($n=8$). Statistical analysis was performed with two-way ANOVA [interaction: $F_{(8,93)}=2.6$; $p<0.01$; row factor: $F_{(4,93)}=1.7$; $p=0.15$; column factor: $F_{(2,93)}=40.6$; $p=0.0001$], followed by Dunnett's *post hoc* test ($n=5$). $**p<0.005$ and $***p<0.001$ shScr+caffeine versus shScr; $*p<0.05$ and $***p<0.001$ shScr+caffeine versus shRyR2+caffeine. (G) Representative images of dendrites from control neurons or from neurons preincubated for 30 min with 10 mM NAC incubated with 10 mM caffeine. (H) Quantification of spine length changes with time determined in control neurons and in neurons preincubated with NAC plus or minus caffeine. Values represent mean \pm SE ($n=8$). Statistical analysis was performed with two-way ANOVA [interaction: $F_{(12,165)}=5.1$; $p=0.0001$; row factor: $F_{(4,165)}=2.3$; $p=0.06$; column factor: $F_{(3,165)}=71.7$; $p=0.0001$], followed by Dunnett's *post hoc* test. $*p<0.01$ and $**p<0.005$ caffeine versus control; $***p<0.001$ caffeine versus caffeine+NAC. Scale bar=2 μm . GFP, green fluorescent protein. To see this illustration in color, the reader is referred to the web version of this article at www.liebertpub.com/ars



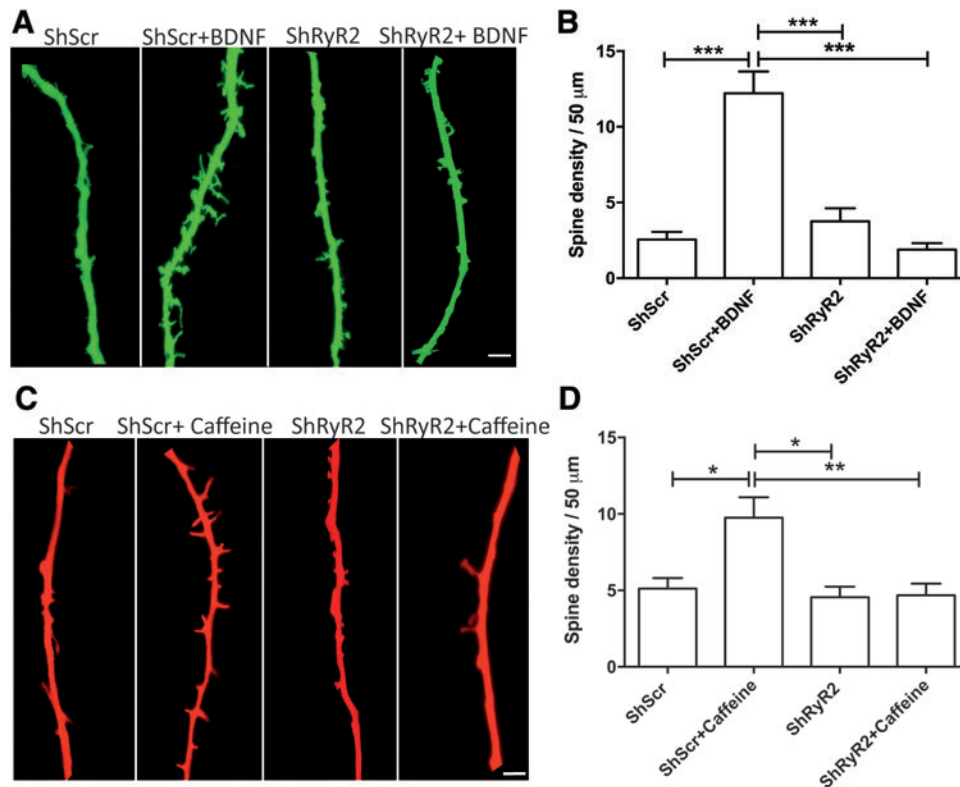


FIG. 7. RyR2 downregulation inhibits long-term dendritic spine remodeling induced by BDNF or caffeine. (A) Representative images of dendrites were acquired after incubation for 6 h with BDNF (50 ng/ml) or vehicle of hippocampal neurons expressing shRyR2 or shScr+GFP. (B) Quantification of spine density determined in neurons expressing shRyR2 or shScr plus or minus BDNF. Values represent mean \pm SE ($n=5$). Statistical analysis of these results was performed with one-way ANOVA ($F=23.0$; $p=0.0001$), followed by Tukey's *post hoc* test ($***p<0.001$). (C) Representative images of dendrites were acquired after 6 h of incubation with 10 mM caffeine or vehicle in hippocampal neurons expressing shRyR2 or shScr+RFP. (D) Spine density quantification in neurons expressing shRyR2 or shScr plus or minus caffeine. Values represent mean \pm SE ($n=5$). Statistical analysis of these results was performed with one-way ANOVA ($F=6.8$; $p=0.002$), followed by Tukey's *post hoc* test ($*p<0.05$; $**p<0.01$). Scale bar = 2 μm . To see this illustration in color, the reader is referred to the web version of this article at www.liebertpub.com/ars

in Fig. 9B) with RyR2-directed antisense oligodeoxynucleotides (ODN-RyR2, 10 nmoles/ μl) or with the scrambled sequence (ODN-Scr, 10 nmol/ μl). These bilateral injections (1 μl each) caused significant downregulation of RyR2 protein contents in the CA1, CA3, and dentate gyrus hippocampal regions, determined by immunohistochemistry analysis (Supplementary Fig. S4) of tissue sections collected 6 h after the ninth training session, but did not affect RyR3 protein levels (Supplementary Fig. S5). Quantification of the immunofluorescence images and Western blot analysis of the whole hippocampus confirmed these findings (Supplementary Fig. S6).

We found that the animals injected with ODN-RyR2 displayed striking defects in the previously memorized spatial task, as indicated by the increased trajectories exemplified in the traces illustrated in Figure 9A, which were collected after the ninth session (see Table in Fig. 9B).

After injection, rats displayed increased ratios of observed over expected distances (Fig. 9C). Statistical analysis of the results presented in Figure 9C was performed with two-way ANOVA [interaction: $F_{(8,90)}=7.4$; $p=0.005$; row factor: $F_{(8,90)}=3.1$; $p<0.0001$; column factor: $F_{(1,90)}=67.4$; $p<0.0001$]. Likewise, after injection, rats displayed increased number of errors along the subsequent sessions (Fig. 9D), analyzed by two-way ANOVA [interaction:

$F_{(8,90)}=32.8$; $p<0.0001$; row factor: $F_{(8,90)}=22.5$; $p<0.0001$; column factor: $F_{(1,90)}=277.0$; $p<0.0001$], followed by Bonferroni's *post hoc* test. Quantification of the number of errors performed in the last session by animals injected with ODN-Scr or ODN-RyR2 revealed significant differences (Fig. 9E), determined by unpaired Student's *t*-test ($***p<0.001$; $n=6$).

Discussion

Summary of results

In this work, we report that RyR2 channels make a major contribution to agonist-induced RyR-mediated Ca^{2+} release in primary hippocampal neurons; NOS or NOX2 inhibitors abolished agonist-induced RyR-mediated Ca^{2+} release, confirming the redox sensitivity of this process. We also show that BDNF-induced RyR2 upregulation and dendritic spine remodeling required RyR2-mediated Ca^{2+} release, H_2O_2 generation, and NOS plus NOX2 activities. Moreover, inhibition of ERK1/2 activity prevented RyR2 upregulation induced by BDNF, whereas selective RyR2 downregulation drastically impaired the capacity of animals to perform a previously memorized spatial memory task.

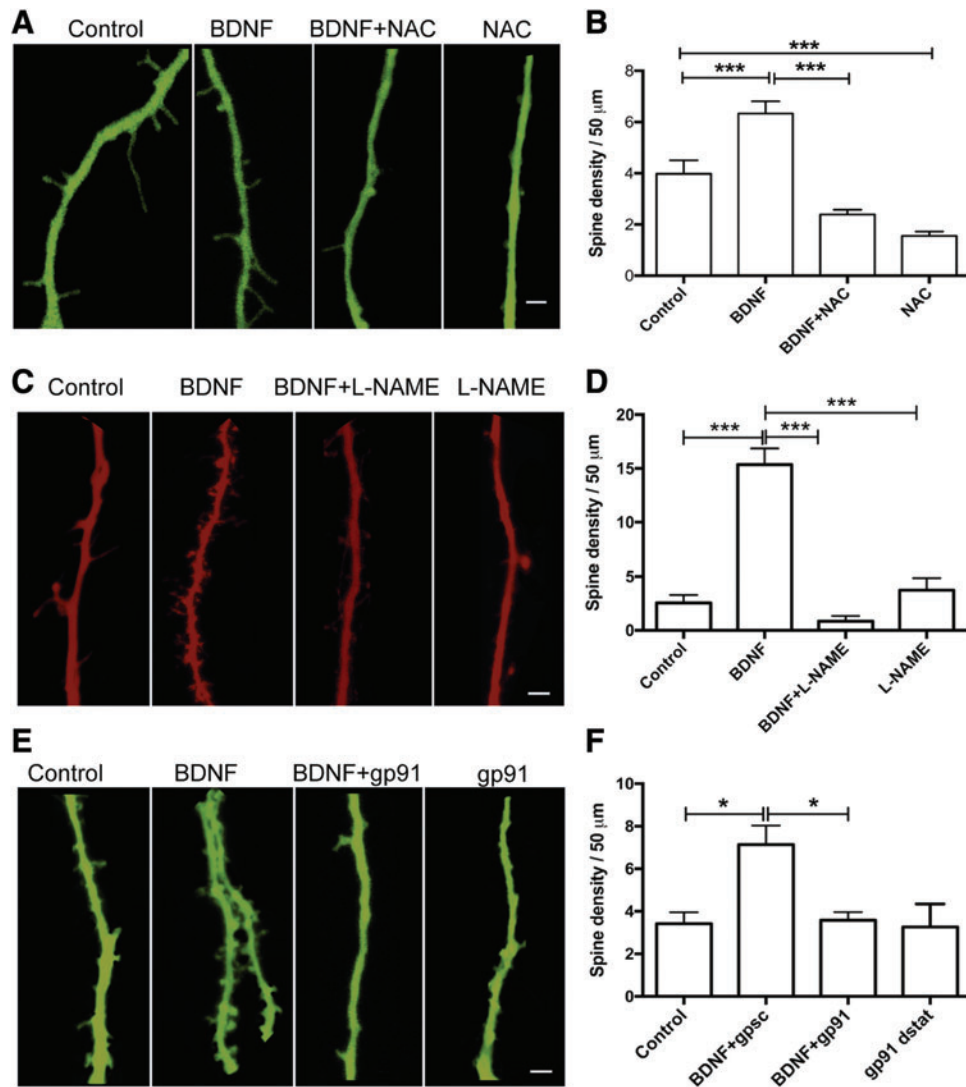


FIG. 8. Long-term structural plasticity induced by BDNF requires NOS and NOX2 ROS generation. (A) Representative images of hippocampal neurites from cultures expressing GFP incubated for 6 h with BDNF (50 ng/ml) or vehicle, plus or minus NAC. Neurons were preincubated for 30 min with 10 mM NAC, which was maintained during the subsequent incubation for 6 h with BDNF or vehicle. (B) Quantification of spine density in control neurons plus or minus BDNF, and in neurons preincubated with NAC plus or minus BDNF. Values represent mean \pm SE ($n=5$). Statistical analysis of the results presented in (B) was performed with one-way ANOVA ($F=38.1$; $p=0.0001$), followed by Tukey's *post hoc* test ($***p<0.001$). (C) Representative images of hippocampal neurites from cultures expressing GFP and incubated for 6 h with vehicle plus or minus gp91 ds-tat, or with BDNF (50 ng/ml) plus gp91 ds-tat or gp91 ds-sc. Cultures were preincubated with these peptides for 30 min, and the peptides were maintained during the 6 h of incubation with BDNF. (D) Quantification of spine density determined in control neurons plus or minus gp91 ds-tat, and in neurons plus RFP incubated with BDNF+gp91 ds-tat or gp91 ds-sc. Values represent mean \pm SE ($n=5$). Statistical analysis of the results presented in (D) was performed with one-way ANOVA ($F=45.1$; $p=0.0001$), followed by Tukey's *post hoc* test ($***p<0.001$). (E) Representative images of hippocampal neurites from cultures expressing RFP and incubated for 6 h with vehicle plus or minus L-NAME, or with BDNF (50 ng/ml) plus or minus L-NAME. Cultures were preincubated with L-NAME (10 μM) for 30 min and L-NAME was maintained during the 6 h of incubation with BDNF. (F) Quantification of spine density determined in control neurons plus or minus BDNF, and in neurons preincubated with L-NAME plus or minus BDNF. Values represent mean \pm SE ($n=4$). Statistical analysis of the results presented in (F) was performed with one-way ANOVA ($F=7.2$; $p=0.015$), followed by Tukey's *post hoc* test ($*p<0.05$). Scale bar = 2 μm . To see this illustration in color, the reader is referred to the web version of this article at www.liebertpub.com/ars

BDNF-induced ROS generation

Previous reports showed that BDNF promotes NO generation in cortical neurons (55, 56, 104). Rat CA1 hippocampal neurons express the NOS enzyme in dendritic spines (21), while incubation of primary hippocampal neurons with

BDNF induces NO generation in both soma and dendrites, in parallel with intracellular Ca^{2+} signals (57). In cortical neurons, BDNF increases the expression levels of the p47 NOX2 subunit, presumably implicating NOX2 as a downstream target of BDNF (54). In this work, we show that ROS generation forms part of the complex array of downstream

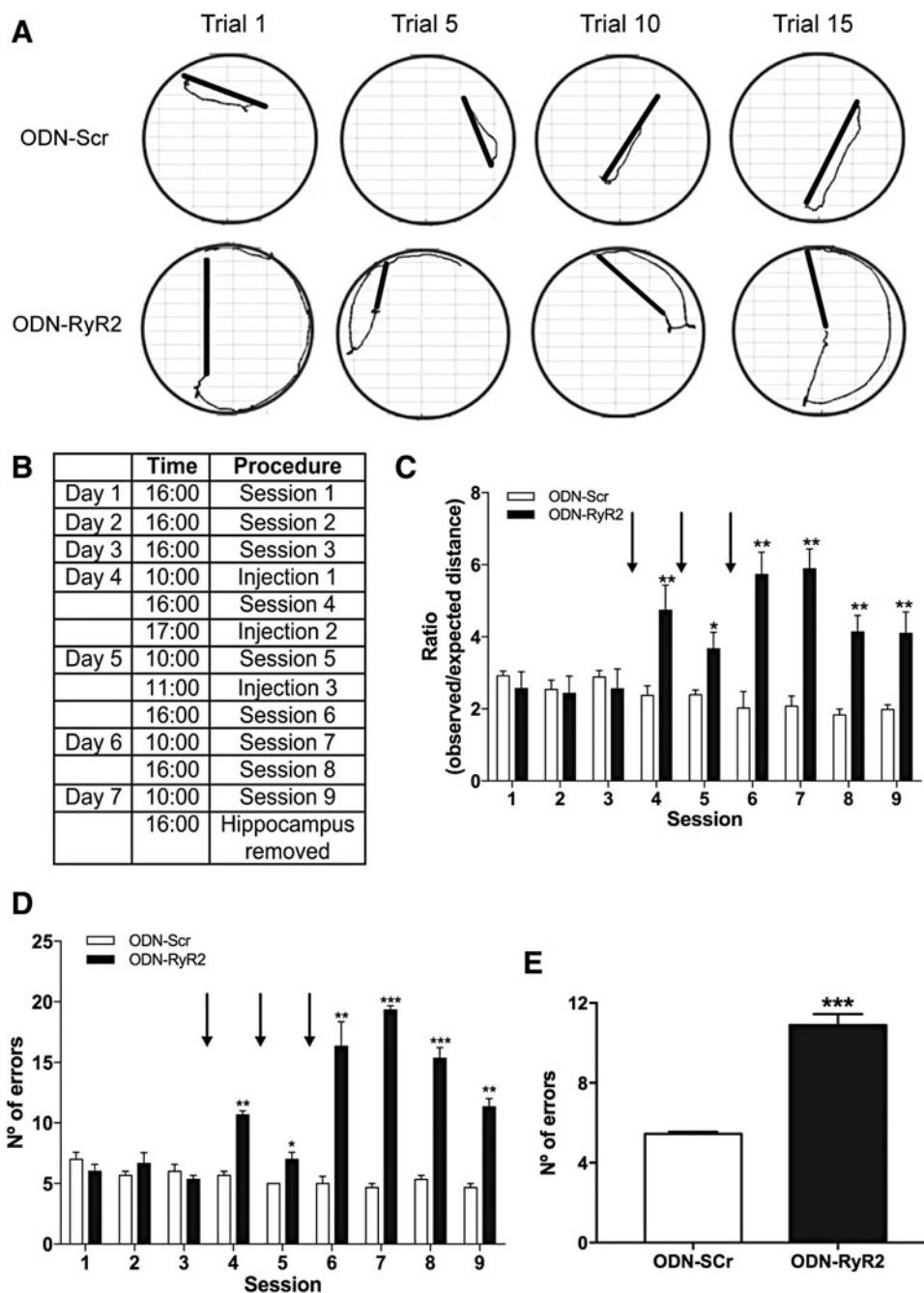


FIG. 9. RyR2 downregulation impairs spatial memory. (A) Walked (*thin lines*) and expected (*shortest*) distances (*thick lines*) to the reward in the arena covered by animals injected with ODN-Scr (*top panels*) or ODN-RyR2 (*lower panels*). Shown are trials 1, 5, 10, and 15 collected from session 9, as defined in (B), which shows the schedule of sessions and injections. (C) Quantification of the ratios between observed/expected distances performed by animals injected bilaterally with 1 μ l per injection of ODN-Scr (10 nmoles/ μ l) or ODN-RyR2 (10 nmoles/ μ l). The injections are indicated by the *arrows*. Values represent mean \pm SE ($n=5$). Statistical analysis of the results presented in (C) was performed with two-way ANOVA [interaction: $F_{(8,90)}=7.4$; $p=0.005$; row factor: $F_{(8,90)}=3.1$; $p<0.0001$; column factor: $F_{(1,90)}=67.4$; $p<0.0001$] Bonferroni *post hoc* test (* $p<0.05$; ** $p<0.01$). (D) Quantification of the number of errors performed by animal injected as above with ODN-Scr or ODN-RyR2; the number of errors represent the times rats visited a well without the reward in each trial. The injections are indicated by *arrows*. Values represent mean \pm SE ($n=5$). Two-way ANOVA [interaction: $F_{(8,90)}=32.8$; $p<0.0001$; row factor: $F_{(8,90)}=22.5$; $p<0.0001$; column factor: $F_{(1,90)}=277.0$; $p<0.0001$], followed by Bonferroni *post hoc* test (** $p<0.01$; *** $p<0.001$). (E) Quantification of the number of errors performed in the last session by animals injected with ODN-Scr or ODN-RyR2. Values represent mean \pm SE ($n=6$). Statistical analysis in (E) was determined by unpaired Student's *t*-test (*** $p<0.001$). ODN-RyR2, RyR2-directed antisense oligodeoxynucleotides; ODN-Scr, scrambled sequence of RyR2-directed antisense oligodeoxynucleotides.

signaling pathways induced by BDNF in hippocampal neurons. In physiological conditions, ROS act as signaling molecules critical for the induction of synaptic plasticity and memory formation (76). Accumulating evidence suggests that there is substantial cross talk between ROS and Ca^{2+} signaling in different cellular systems (34,117), including hippocampal neurons (41). Here, we found that inhibition of NMDA receptors or RyR2 downregulation prevented BDNF-induced cytoplasmic H_2O_2 generation. Accordingly, we propose that Ca^{2+} signals initially produced by Ca^{2+} influx via NMDA receptors, and subsequently amplified through RyR2-mediated CICR, are essential for BDNF-induced ROS generation, presumably by enhancing NOS activation by Ca^{2+} .

Previous studies indicate that hippocampal neurons express the NOX2 enzyme (111), and that activation of NMDA receptors results in sequential activation of NOS and NOX2 in neocortical neuronal cultures (33). Here, we found that BDNF-induced cytoplasmic H_2O_2 generation required both NOS and NOX activities. Previous reports indicate that NOS-generated nitric oxide enhances RyR activity via *S*-nitrosylation of RyR cysteine residues (109); however, ROS-induced RyR redox modifications, and not RyR *S*-nitrosylation, are required for brain RyR channel stimulation promoted by increased

cellular oxidative conditions (20). Our results show that PKG inhibition suppressed BDNF-induced ROS generation. Hence, we propose that BDNF triggers a signaling cascade that engages sequentially NMDA receptors, NOS, PKG, and NOX2 enzymes, and redox-sensitive RyR2-mediated CICR, as illustrated in the scheme presented in Figure 10.

BDNF-induced RyR2 upregulation

Here, we show that RyR2 downregulation prevented Ca^{2+} release induced by 4-CMC, a strong indication that the RyR2 isoform is mostly responsible for this response. RyR2 downregulation hindered BDNF-induced RyR2 upregulation as well, suggesting that RyR2-mediated Ca^{2+} release is a key factor for its own expression. In addition, we found that the enhanced RyR2 expression induced by BDNF required ERK1/2 activity, which has a key role in the synaptic plasticity processes elicited by BDNF (4). Moreover, ERK1/2 activity is essential for the activation of the transcription factor cAMP response element-binding (CREB), which is central for long-term hippocampal synaptic plasticity and spatial memory processes (7). Nicotine administration to mice upregulates RyR2 levels in a number of brain areas associated with cognition and addiction, such as the cortex and ventral midbrain; RyR2 upregulation requires CREB activation via a mechanism dependent on CICR (122).

Future studies should address if BDNF-induced RyR2 upregulation involves CREB activation in hippocampal neurons. In addition, we found that the antioxidant NAC, or NOS or NOX2 inhibition, prevented BDNF-induced RyR2 upregulation. We suggest that cross talk between RyR2-mediated Ca^{2+} and ROS signaling plays a key role in RyR2 upregulation induced by BDNF.

BDNF-induced dendritic spine remodeling

Dendritic spines are miniature protrusions that compose most excitatory synapses in the mammalian brain [reviewed in Lippman and Dunaevsky (71) and Nimchinsky *et al.* (86)]. These structures receive, integrate, and compartmentalize the immense majority of excitatory inputs (37, 86). The shape and numbers of spines are a direct consequence of changes in neuronal activity (15, 112), which engages different Ca^{2+} signaling pathways (39, 42, 103). Dendritic spine remodeling, including the formation/elongation and the pruning/retraction of spines, requires changes in intracellular Ca^{2+} concentration (87), which are necessary for the actin-mediated spine enlargement associated with electrical stimulation (30, 87, 114). Previous work demonstrated that BDNF has an essential role in the structural remodeling of excitatory synapses (3, 4, 113). In brain slices, the gradual spine enlargement induced specifically by synaptic stimulation strongly depends on protein synthesis and BDNF signaling (110). Dendritic spine size positively correlates with an increase in AMPA-receptor-mediated currents at stimulated synapses and depends on NMDA receptors, calmodulin and actin polymerization (77, 78). In young hippocampal synapses, increased or decreased spine sizes, respectively, occur during persistent LTP or long-term depression (78, 82, 89, 120). Spontaneously released glutamate is sufficient to activate nearby spines, which can then lead to the growth of new postsynaptic processes connecting to a presynaptic site (100). Similarly, in cultured hippocampal neurons, short pulses of glutamate applied to

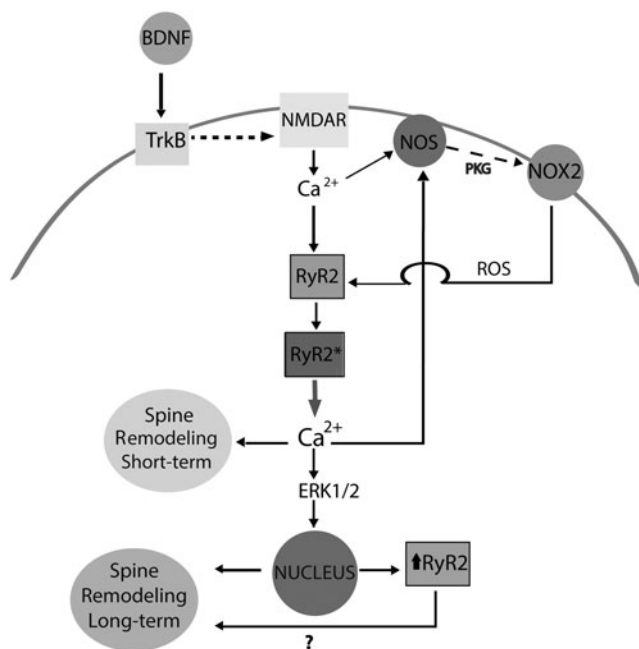


FIG. 10. Scheme of the model proposed to account for RyR2-dependent spine remodeling and RyR2 upregulation. The figure illustrates a model through which BDNF binding to its membrane receptor TrkB triggers a signaling cascade that engages sequentially NMDA receptors and the NOS, PKG, and NOX2 enzymes, resulting in increased ROS generation. The increase in Ca^{2+} produced by NMDA receptor activation together with NOX2-generated ROS enhances RyR2 activity, indicated as RyR2* in the figure. The resulting enhanced Ca^{2+} signaling, generated via redox-dependent CICR, promotes short- and long-term spine remodeling, the latter via Ca^{2+} -dependent ERK1/2 activation, and results in RyR2 upregulation. The question mark illustrated in the scheme reflects that it is not known whether RyR2 upregulation contributes to long-term spine remodeling. CICR, Ca^{2+} -induced Ca^{2+} release.

dendrites induce spine elongation, whereas long pulses cause shrinking (59).

One of the main findings of our work is the strong dependence of BDNF-induced dendritic spine remodeling on RyR2-mediated Ca^{2+} release and ROS generation *via* NOS/NOX2. These results, which add to previous work (1, 58), show for the first time that BDNF-induced ROS generation is important for the structural remodeling of dendritic spines induced by BDNF. In addition, RyR2-mediated Ca^{2+} signals also mediated BDNF-induced dendritic spine remodeling, highlighting that the cross talk between Ca^{2+} and ROS signaling is a central process in activity-dependent neuronal function. In fact, ROS signaling and RyR-mediated Ca^{2+} release are key activities for neuronal polarization (115).

RyR2 downregulation impairs spatial memory

The involvement of RyR channels in the generation of postsynaptic Ca^{2+} signals, synaptic plasticity, and memory processes has acquired increasing relevance in the last two decades (8, 28, 29, 31, 74, 81, 97, 99, 101, 119). In chickens trained in a passive avoidance discrimination task, treatment with dantrolene to inhibit RyR channel activity causes loss of memory retention (28), while administration of the RyR agonist 4-CMC enhances memory consolidation (8). In mice conditioned in an inhibitory avoidance task (31), or trained in a radial arm-maze task (88), RyR channel inhibition with dantrolene or with high concentrations of ryanodine alters memory retention. In contrast, intrahippocampal injection of stimulatory ryanodine enhances both learning and memory consolidation in rats trained in the Morris water maze (1). Selective knockdown by intracerebrovascular injection of antisense ODNs of the RyR2 and the RyR3 isoforms in mice, but not of the RyR1 isoform, impairs memory retention in a passive avoidance test (31).

Here, we report that injection in the hippocampal CA1 region of a specific ODN anti-RyR2 caused severe defects in a spatial task previously memorized by rats. Remarkably, rats exhibited utter disorientation after downregulation of RyR2 expression, while injection of the scrambled ODN did not affect the memorized behavior. These results highlight the relevance of RyR2 expression for successful performance of hippocampal-dependent spatial tasks. Furthermore, rodent exposure to different hippocampal-dependent memory tasks, including the Morris water maze (1, 119) and novel object recognition (6), results in significant RyR2 upregulation and in less prominent RyR3 upregulation as well. Based on these combined findings, it seems reasonable to propose that hippocampal-dependent memory formation and consolidation not only require RyR2 channel expression but also entail $\text{RyR2} > \text{RyR3}$ upregulation to ensure the generation of the Ca^{2+} signals required for memory processes.

It is worth mentioning that sublethal concentrations of soluble amyloid β -peptide oligomers ($A\beta$ Os), increasingly recognized as causative agents of Alzheimer's disease, decrease RyR2 protein content and prevent BDNF- or caffeine-induced spine remodeling (92). The significant RyR2 protein downregulation induced by $A\beta$ Os may contribute to the RyR decrease reported in Alzheimer's patients at early stages of the disease (51). Hence, RyR2 downregulation may represent a significant factor in the impaired synaptic plasticity and memory defects characteristic of this neurodegenerative disorder.

Materials and Methods

Materials

BDNF and 4-CMC were from Merck Millipore (Darmstadt, Germany). Fluo4-AM, calcein-AM, Alexa Fluor[®] 488, TRIzol reagent Hoechst 33258, GlutaMAX[™], and Lipofectamine 2000 transfection reagent were from Invitrogen (Carlsbad, CA). DAKO mounting medium and Brilliant III Ultra-Fast SYBR[®] GREEN qPCR Master Mix were from Agilent Technologies (Santa Clara, CA). Ryanodine was from Tocris Bioscience (Bristol, United Kingdom). N-acetyl-L-cysteine, L-NAME, and MK801 were from Sigma-Aldrich (Darmstadt, Germany). KT-5823 was from Tocris Bioscience. Gp91ds-tat and gpcr were from Anaspec (Fremont, CA). B27 supplement and Neurobasal medium were from Gibco (Carlsbad, CA). Mounting solution for slide coating was from Vectashield (Vector Laboratories, Burlingame, CA).

Mouse anti-RyR2 (MA3-916) was from Thermo Fisher. Rabbit anti-RyR3 (AB9082) was from Merck Millipore, and monoclonal anti- β actin (A5316) from Sigma-Aldrich (St. Louis, MO). A highly selective RyR1 antibody was kindly provided by Dr. Vincenzo Sorrentino. DNAase digestion (DNA-free[™] Kit) was obtained from Ambion (Austin, TX), and ImProm-II Reverse Transcriptase kit was from Promega (Madison, WI). PVDF membranes (Trans-Blot[®] Turbo Mini PVDF) were from Bio-Rad Laboratories (Hercules, CA). The amplification system MX3000P was from Stratagene (La Jolla, CA). The pRFP-C-RS and pRFP-C-RS (TR30014) vectors and plasmid containing a noneffective 29-mer shScr cassette (TR30013 and TR30015) were from Origene (Rockville, MA). The HyPer[™]-Cyto plasmid was from Evrogen (Moscow, Russia).

Primary rat hippocampal cultures

Primary cultures were prepared from the hippocampus dissected from Sprague-Dawley rats at embryonic day 18 (1, 92). Cells were plated in minimum essential medium plus 10% horse serum for 40 min to allow adhesion of neurons and minimize glial cell adhesion. Cultures were maintained subsequently at 37°C under 5% CO_2 in serum-free Neurobasal medium supplemented with B27 serum free and 2 mM GlutaMAX. Hippocampal cultures were used at 14 days *in vitro* (DIV) for all experiments.

All experimental protocols used in this work complied with the "Guiding Principles for Research Involving Animals and Human Beings" of the American Physiological Society and were approved by the Bioethics Committee on Animal Research, Faculty of Medicine, Universidad de Chile.

Transfection with knockdown plasmid vectors

Cells in primary culture were transiently transfected with Lipofectamine 2000 according to the manufacturer's specifications. Neurons were transfected with 1 μl Lipofectamine-2000 in Neurobasal medium containing 2 μg of shRNA expression vector specific to silence RyR2 expression. This shRNA expression vector was obtained by cloning a shRNA cassette directed against rat RyR2 mRNA (target sequence 5'-AGGAAGCAATGGTGGACAAGTTGGCTGAA-3') in the BamHI/HindIII cloning sites of pGFP-V-RS vector or pRFP-C-RS vector. A plasmid containing a noneffective 29-mer shScr cassette (TR30013 and TR30015) was used as

control. One day post-transfection, cultures were stimulated with BDNF (50 ng/ml) as described in the text to perform experiment of RyR2 expression or spine remodeling.

RNA isolation and real time PCR

Total RNA was isolated using TRIzol reagent; DNase digestion was included to remove any contaminating genomic DNA. RNA purity was assessed by the 260/280 absorbance ratio and RNA integrity by gel electrophoresis. Complementary DNA (cDNA) was synthesized with 1 μ g total RNA with the Improm TM II reverse transcriptase. One hundred nanograms of cDNA was used in 20 μ l final volume for qPCR amplification. qPCR was performed in an amplification system (MX3000P; Stratagene) using the Brilliant III Ultra-Fast SYBR GREEN qPCR Master Mix. Amplification was performed after 35 cycles, each of which included 15 s at 95°C, 15 s at 60°C (RyR2 and β -actin), and 15 s at 72°C. After these cycles, a final 15-s incubation step at 95°C was added. Primers (1) were as follows (f: forward; r: reverse): RyR1 f 5'-GCCTTTGATGTGGGATTACAG-3'; r 5'-CCCCAACTCGAACCTTCTCTC-3'. RyR2 f 5'-AATCAAAGTGGCGGAATTTCTTG-3'; r 5'-TCTCCCTCAGCCTTCTCCGGTTC-3'. RyR3 f 5'-GAAGCCTGTTGGTGGACCATAC-3'; r 5'-TCCAGAGTGTTCGATAAAGGAG-3'. β -actin f 5'-TCTACAATGAGCTGCGTGTG-3'; β -actin r 5'-TACATGGCTGGGGTGTGAA-3'. The levels of RyR mRNA were assessed with the $2^{-\Delta\Delta CT}$ method (95) using β -actin as housekeeping gene. Dissociation curves were analyzed to verify purity of products. All samples, including controls, were run in triplicate.

Western blot analysis

Cells extracts prepared as described (52) were resolved by sodium dodecyl sulfate/polyacrylamide gel electrophoresis (4% with a base of 15% polyacrylamide gels), transferred to PDVF membranes, and incubated overnight with specific antibodies against RyR2. To correct for loading, membranes were stripped and reprobed for β -actin using a specific antibody. The image acquisition and densitometric analysis of band density were performed by means of the ChemiDocTM MP System and the Image Lab software by Bio-Rad Laboratories, respectively.

Immunofluorescence

Hippocampal cultures transfected with shRyR2 or shScr were fixed by adding an equal volume of 4% paraformaldehyde and Neurobasal medium for 5 min. After replacing this medium with a solution containing 4% paraformaldehyde, cultures were incubated for 10 min and washed with phosphate-buffered saline (PBS) at pH 7.4. Fixed cultures were incubated for 2 h with a blocking and permeabilization solution containing 3% donkey serum and 0.25% Triton X-100 (in PBS 1 \times); next, cultures were incubated overnight at 4°C with primary antibody anti-RyR2 diluted in blocking solution. After this incubation period, cultures were washed with PBS and incubated for 2 h with the secondary antibody Alexa Fluor 488 anti-rabbit (in blocking solution) at room temperature. Cultures were washed with PBS, and coverslips were mounted in DAKO mounting medium for microscope observation. Cells were visualized in a Nikon C2+ confocal microscope (Melville, NY), with the 63 \times objective lens. Images were analyzed using ImageJ software (National Institutes of Health).

Immunohistochemistry

Brain tissue fixation and immunohistochemistry were performed as described (1). Briefly, each animal was perfused transcardially and under anesthesia with saline solution (NaCl 0.9%), followed by 4% paraformaldehyde in 0.1 M phosphate buffer, pH 7.4, to fix and remove their brains. Brains were postfixed for 2 h in paraformaldehyde and were cryopreserved in PBS containing 30% sucrose plus 0.03% sodium azide for subsequent slice preparation with a microtome. Coronal slices (40 μ m) were incubated in the blocking/permeabilization solution for 2 h at room temperature, and were then incubated overnight at 4°C in blocking/permeabilization solution under shaking with anti-RyR2 or anti-RyR3 primary antibodies, diluted to 1:50 and 1:100, respectively. Slices were washed three times for 5 min with PBS, followed by a 5-min wash with blocking/permeabilization solution before further incubation with the secondary antibodies Alexa 488 goat anti-mouse and Alexa 488 chicken anti-rabbit, respectively. Slices were then washed three times with PBS, for 10 min at room temperature, and then incubated with Hoechst 33258 for detection of the cell nucleus for 5 min at room temperature. Slices were mounted on slides coated with mounting solution to preserve fluorescence. The ImageJ software program was used for image analysis and generation of zeta projections from stacks (1.5 mm thickness each). Total intensity of RyR2 or RyR3 fluorescence in each z-projection was measured and normalized by Hoechst fluorescence intensity.

Determination of cytoplasmic Ca²⁺ signals

Cells were transferred to modified Tyrode's solution (in mM: 129 NaCl, 5 KCl, 2 CaCl₂, 1 MgCl₂, 30 glucose, and 25 HEPES, pH 7.3), preloaded for 30 min at 37°C with 2.5 μ M Fluo-4 AM, and washed for 10 min in modified Tyrode's solution to allow complete dye de-esterification. Fluorescence images of intracellular Ca²⁺ signals in primary hippocampal neurons (14 DIV) were obtained every 5 s with an inverted confocal microscope (Axiovert 200, LSM 5 Pascal; Carl Zeiss, Oberkochen, Germany), using Plan Apochromat 63 \times Oil DIC objective (excitation at 488 nm, argon laser beam). Image data were acquired from different regions of optical interest located in the cell bodies. Frame scans were averaged using the equipment data acquisition program. Fluorescence signals are shown as F/F_0 values, where F_0 corresponds to the basal fluorescence recorded before any treatment. The increase in fluorescence induced by 0.5 mM 4-CMC did not saturate the probe, as tested by addition of ionomycin at the end of the experiment (2). All experiments were done at room temperature (20–22°C).

Determination of H₂O₂

Hippocampal neurons were transiently transfected with the HyPer-Cyto plasmid at 14 DIV. This plasmid codes for a cytoplasmic protein, HyPer-Cyto, which has a circularly permuted yellow fluorescent protein inserted into the regulatory domain of the prokaryotic H₂O₂-sensing protein OxyR (12), allowing selective detection of H₂O₂ production in living cells. One day post-transfection, cells were washed with Tyrode's solution and were stimulated with BDNF 50 ng/ml in the same solution. Images were obtained every 5 s with an inverted

confocal microscope (Axiovert 200, LSM 5 Pascal; Carl Zeiss) using the Plan Apochromat 63× Oil DIC objective (excitation at 488 nm, argon laser beam). Changes in probe fluorescence, which reflect H₂O₂ levels, are presented as F/F_0 values, where F_0 corresponds to the average basal fluorescence obtained from a specific interest region in the soma.

Morphological analysis of dendritic spines

We analyzed the changes in spine morphology by confocal microscopy of hippocampal cultures (14 DIV). Confocal fluorescence images were obtained with a Zeiss LSM-5, Pascal 5 Axiovert 200 microscope, by using LSM 5.3.2 image capture and analysis software and a Plan-Apochromat 63×/1.4 Oil DIC objective. Dendrites in 30–50 μm proximity to the soma were selected randomly independently of their spine density. We used the ImageJ software program for image deconvolution and zeta-projection reconstruction from 10 to 15 stacks (0.4 μm each) to measure spine length. Spine density in dendrites was analyzed by measuring the number of spines present in a length of 50 μm; five dendrites were analyzed per condition in five independent experiments. Short-term changes were monitored for 1 h after BDNF incubation through acquisition of dendrite images every 15 min; long-term changes were visualized after 6 h of incubation with BDNF. We used two different strategies to visualize cellular morphology; neurons were loaded for 20 min with 1 μM calcein-AM in Tyrode's solution or neurons were transfected with pGFP-V-RS or pRFP-C-RS vectors that express the green fluorescent protein (GFP) or the RFP, respectively, coupled to the expression of shRyR2. Transfection with the scrambled sequence or only with the RFP or GFP was used as control.

Spatial memory evaluation

Bilateral injections of ODN-RyR2 or ODN-Scr were performed into rat CA1 hippocampal region. Two-month-old Sprague-Dawley male rats (250–280 g) were anesthetized with isoflurane (3% in oxygen) for induction of anesthesia. Isoflurane (2% in oxygen) was also used for maintenance of anesthesia, at a constant oxygen flow (1 L/min). Two 21-gauge stainless steel guide cannulas were implanted bilaterally in the CA1 hippocampal region of each rat. Target coordinates, calculated as given in Ref. (94), were as follows relative to bregma: anteroposterior –3.30, lateral ±2.6 mm, 1.8 mm in depth, with 10° angles to target the dorsal CA1 hippocampal region. Guide cannulas were fixed to the skull with skull screws and dental cement. Following surgery, animals were individually housed with food and water *ad libitum* for 7 days before exposure to the Oasis maze task, a modified dry-land version of the Morris water maze (25, 53).

To evaluate hippocampal-dependent spatial learning, cannulated and water-deprived pretrained animals were trained and tested during three consecutive daily sessions in the Oasis maze task, which involved searching for the reward (water) placed in the same one of 21 equidistant wells on a circular arena provided with visual cues; each session was composed of 15 trials of 1-min duration each. After this initial training period, animals received three bilateral injections (1.0 μl each) of ODN-RyR2 (10 nmoles/μl) or ODN-Scr (10 nmoles/μl), with the following sequences. ODN-RyR2: 5'T*T*CGCCCGCATCAGCC*A*T-

3'; ODN-Scr: 5'C*G*GCAGGAGTCTGTGC*G*C-3', the * indicates the phosphorothioate residues.

A complete scheme of training sessions and injections is illustrated in the Table presented in Figure 9B. Animal behavior was recorded with a video camera in the zenithal position. Video recordings were analyzed using the Virtual Dub software. The position of the animal was tracked and navigation was reconstructed and analyzed with a MATLAB (MathWorks) routine. Six hours after the conclusion of session 9, animals were perfused and their brains were removed and sliced in a frozen microtome for immunohistochemistry analysis of RyR2 and RyR3 (for details, see the Immunohistochemistry section). Fluorescence images, captured in an inverted confocal microscope C2+ Spectral Nikon Eclipse TI, were analyzed with the ImageJ software.

Statistics

Results are expressed as mean ± SE from at least three independent experiments. Statistical significance was evaluated with the GraphPad Prism 7.0 Software (San Diego, CA). The particular analysis performed in each case, Student's *t*-test, one-way or two-way ANOVA, is detailed in the Results section and figure legends.

Acknowledgments

We thank Dr. Vincenzo Sorrentino, University of Siena, Italy, for his kind gift of a highly specific RyR1 antibody. This work was supported by FONDECYT (3120093, 11140580, 1140545, 1150736, and 1170053) and by BNI (P-09-015).

Author Disclosure Statement

No competing financial interests exist.

References

- Adasme T, Haeger P, Paula-Lima AC, Espinoza I, Casas-Alarcón MM, Carrasco MA, and Hidalgo C. Involvement of ryanodine receptors in neurotrophin-induced hippocampal synaptic plasticity and spatial memory formation. *Proc Natl Acad Sci U S A* 108: 3029–3034, 2011.
- Adasme T, Paula-lima A, and Hidalgo C. Inhibitory ryanodine prevents ryanodine receptor-mediated Ca²⁺ release without affecting endoplasmic reticulum Ca²⁺ content in primary hippocampal neurons. *Biochem Biophys Res Commun* 458: 57–62, 2015.
- Alonso M, Vianna MR, Depino AM, Mello e Souza T, Pereira P, Szapiro G, Viola H, Pitossi F, Izquierdo I, and Medina JH. BDNF-triggered events in the rat hippocampus are required for both short- and long-term memory formation. *Hippocampus* 12: 551–560, 2002.
- Alonso M, Medina JH, and Pozzo-miller L. ERK1/2 activation is necessary for BDNF to increase dendritic spine density in hippocampal CA1 pyramidal neurons. *Learn Mem* 11: 172–178, 2004.
- Amaral MD and Pozzo-Miller L. BDNF induces calcium elevations associated with IBDNF, a nonselective cationic current mediated by TRPC channels. *J Neurophysiol* 98: 2476–2482, 2007.
- Arias-Cavieres A, Adasme T, Sánchez G, Muñoz P, and Hidalgo C. Aging impairs hippocampal-dependent recognition memory and LTP and prevents the associated RyR up-regulation. *Front Aging Neurosci* 9: 1–16, 2017.

7. Bading H. Nuclear calcium signalling in the regulation of brain function. *Nat Rev Neurosci* 14: 593–608, 2013.
8. Baker KD, Edwards TM, and Rickard NS. A ryanodine receptor agonist promotes the consolidation of long-term memory in young chicks. *Behav Brain Res* 206: 143–146, 2010.
9. Baker KD, Edwards TM, and Rickard NS. The role of intracellular calcium stores in synaptic plasticity and memory consolidation. *Neurosci Biobehav Rev* 37: 1211–1239, 2013.
10. Balkowiec A and Katz DM. Cellular mechanisms regulating activity-dependent release of native brain-derived neurotrophic factor from hippocampal neurons. *J Neurosci* 22: 10399–10407, 2002.
11. Bekinschtein P, Cammarota M, Izquierdo I, Medina JH, Izquierdo I, and Medina JH. Persistence of long-term memory storage requires a late protein synthesis- and BDNF-dependent phase in the hippocampus. *Neuron* 53: 261–277, 2007.
12. Belousov VV, Fradkov AF, Lukyanov KA, Staroverov DB, Shakhbazov KS, Tersikh AV, and Lukyanov S. Genetically encoded fluorescent indicator for intracellular hydrogen peroxide. *Nat Methods* 3: 281–286, 2006.
13. Berridge MJ. Neuronal calcium signaling. *Neuron* 21: 13–26, 1998.
14. Bibel M and Barde YA. Neurotrophins: key regulators of cell fate and cell shape in the vertebrate nervous system. *Genes Dev* 14: 2919–2937, 2000.
15. Bloodgood BL, Giessel AJ, and Sabatini BL. Biphasic synaptic Ca influx arising from compartmentalized electrical signals in dendritic spines. *PLoS Biol* 7: e1000190, 2009.
16. Blum R and Konnerth A. Neurotrophin-mediated rapid signaling in the central nervous system: mechanisms and functions. *Physiology (Bethesda)* 20: 70–78, 2005.
17. Blum R, Kafitz KW, and Konnerth A. Neurotrophin-evoked depolarization requires the sodium channel NaV1.9. *Nature* 419: 687–693, 2002.
18. Bolton MM, Pittman AJ, and Lo DC. Brain-derived neurotrophic factor differentially regulates excitatory and inhibitory synaptic transmission in hippocampal cultures. *J Neurosci* 20: 3221–3232, 2000.
19. Bramham CR and Messaoudi E. BDNF function in adult synaptic plasticity: the synaptic consolidation hypothesis. *Prog Neurobiol* 76: 99–125, 2005.
20. Bull R, Finkelstein JP, Gálvez J, Sánchez G, Donoso P, Behrens MI, and Hidalgo C. Ischemia enhances activation by Ca²⁺ and redox modification of ryanodine receptor channels from rat brain cortex. *J Neurosci* 28: 9463–9472, 2008.
21. Burette A, Zabel U, Weinberg RJ, Schmidt HH, and Valtschanoff JG. Synaptic localization of nitric oxide synthase and soluble guanylyl cyclase in the hippocampus. *J Neurosci* 22: 8961–8970, 2002.
22. Carmignoto G, Pizzorusso T, Tia S, and Vicini S. Brain-derived neurotrophic factor and nerve growth factor potentiate excitatory synaptic transmission in the rat visual cortex. *J Physiol* 498: 153–164, 1997.
23. Caroni P, Donato F, and Muller D. Structural plasticity upon learning: regulation and functions. *Nat Rev Neurosci* 13: 478–490, 2012.
24. Citri A and Malenka RC. Synaptic plasticity: multiple forms, functions, and mechanisms. *Neuropsychopharmacology* 33: 18–41, 2008.
25. Clark RE, Broadbent NJ, and Squire LR. Hippocampus and remote spatial memory in rats. *Hippocampus* 15: 260–272, 2005.
26. Crozier RA, Black IB, and Plummer MR. Blockade of NR2B-containing NMDA receptors prevents BDNF enhancement of glutamatergic transmission in hippocampal neurons. *Learn Mem* 6: 257–266, 1999.
27. Edelmann E, Cepeda-Prado E, Franck M, Lichtenecker P, Brigadski T, and Leßmann V. Theta burst firing recruits BDNF release and signaling in postsynaptic CA1 neurons in spike-timing-dependent LTP. *Neuron* 86: 1041–1054, 2015.
28. Edwards TM and Rickard NS. Pharmacological evidence indicating a complex role for ryanodine receptor calcium release channels in memory processing for a passive avoidance task. *Neurobiol Learn Mem* 86: 1–8, 2006.
29. Emptage N, Bliss TV, and Fine A. Single synaptic events evoke NMDA receptor-mediated release of calcium from internal stores in hippocampal dendritic spines. *Neuron* 22: 115–124, 1999.
30. Fifková E. A possible mechanism of morphometric changes in dendritic spines induced by stimulation. *Cell Mol Neurobiol* 5: 47–63, 1985.
31. Galeotti N, Quattrone A, Vivoli E, Norcini M, Bartolini A, and Ghelardini C. Different involvement of type 1, 2, and 3 ryanodine receptors in memory processes. *Learn Mem* 15: 315–323, 2008.
32. Giannini G, Conti A, Mammarella S, and Scrobogna M. The ryanodine receptor/calcium channel genes are widely and differentially expressed in murine brain and peripheral tissues. *J Cell Biol* 128: 893–904, 1995.
33. Girouard H, Wang G, Gallo EF, Anrather J, Zhou P, Pickel VM, and Iadecola C. NMDA receptor activation increases free radical production through nitric oxide and NOX2. *J Neurosci* 29: 2545–2552, 2009.
34. Gordeeva AV, Zvyagilskaya RA, and Labas YA. Cross talk between reactive oxygen species and calcium in living cells. *Biochemistry (Mosc)* 68: 1077–1080, 2003.
35. Görlach A, Bertram K, Hudcova S, and Krizanová O. Calcium and ROS: a mutual interplay. *Redox Biol* 6: 260–271, 2015.
36. Gottmann K, Mittmann T, and Lessmann V. BDNF signaling in the formation, maturation and plasticity of glutamatergic and GABAergic synapses. *Exp Brain Res* 199: 203–234, 2009.
37. Harris K and Kater SB. Dendritic spines: cellular specializations imparting both stability and flexibility to synaptic function. *Annu Rev Neurosci* 17: 341–371, 1994.
38. Hartmann M, Heumann R, and Lessmann V. Synaptic secretion of BDNF after high-frequency stimulation of glutamatergic synapses. *EMBO J* 20: 5887–5897, 2001.
39. Hayashi Y and Majewska AK. Dendritic spine geometry: functional implication and regulation. *Neuron* 46: 529–532, 2005.
40. He J, Gong H, and Luo Q. BDNF acutely modulates synaptic transmission and calcium signalling in developing cortical neurons. *Cell Physiol Biochem* 16: 69–76, 2005.
41. Hidalgo C and Donoso P. Crosstalk between calcium and redox signaling: from molecular mechanisms to health implications. *Antioxid Redox Signal* 10: 1275–1312, 2008.
42. Holcman D, Schuss Z, and Korkotian E. Calcium dynamics in dendritic spines and spine motility. *Biophys J* 87: 81–91, 2004.

43. Holtmaat A and Svoboda K. Experience-dependent structural synaptic plasticity in the mammalian brain. *Nat Rev Neurosci* 10: 759, 2009.
44. Huang EJ and Reichardt LF. Trk receptors: roles in neuronal signal transduction. *Annu Rev Biochem* 72: 609–642, 2003.
45. Itami C, Kimura F, Kohno T, Matsuoka M, Ichikawa M, Tsumoto T, and Nakamura S. Brain-derived neurotrophic factor-dependent unmasking of “silent” synapses in the developing mouse barrel cortex. *Proc Natl Acad Sci U S A* 100: 13069–13074, 2003.
46. Johenning FW, Theis AK, Pannasch U, Rückl M, Rüdiger S, and Schmitz D. Ryanodine receptor activation induces long-term plasticity of spine calcium dynamics. *PLoS Biol* 13: e1002181, 2015.
47. Kafitz KW, Rose CR, Thoenen H, and Konnerth A. Neurotrophin-evoked rapid excitation through TrkB receptors. *Nature* 401: 918–921, 1999.
48. Kamsler A and Segal M. Hydrogen peroxide as a diffusible signal molecule in synaptic plasticity. *Mol Neurobiol* 29: 167–178, 2004.
49. Kamsler A and Segal M. Paradoxical actions of hydrogen peroxide on long-term potentiation in transgenic superoxide dismutase-1 mice. *J Neurosci* 23: 10359–10367, 2003.
50. Kang H and Schuman EM. A requirement for local protein synthesis in neurotrophin-induced hippocampal synaptic plasticity. *Science* 273: 1402–1406, 1996.
51. Kelliher M, Fastbom J, Cowburn RF, Bonkale W, Ohm TG, Ravid R, Sorrentino V, and O’Neill C. Alterations in the ryanodine receptor calcium release channel correlate with Alzheimer’s disease neurofibrillary and β -amyloid pathologies. *Neuroscience* 92: 499–513, 1999.
52. Kemmerling U, Muñoz P, Müller M, Sánchez G, Aylwin ML, Klann E, Carrasco MA, and Hidalgo C. Calcium release by ryanodine receptors mediates hydrogen peroxide-induced activation of ERK and CREB phosphorylation in N2a cells and hippocampal neurons. *Cell Calcium* 41: 491–502, 2007.
53. Kesner RP, Farnsworth G, and Kametani H. Role of parietal cortex and hippocampus in representing spatial information. *Cereb Cortex* 1: 367–373, 1991.
54. Kim SH, Won SJ, Sohn S, Kwon HJ, Lee JY, Park JH, and Gwag BJ. Brain-derived neurotrophic factor can act as a proneurotrophic factor through transcriptional and translational activation of NADPH oxidase. *J Cell Biol* 159: 821–831, 2002.
55. Klöcker N, Cellierino A, and Bähr M. Free radical scavenging and inhibition of nitric oxide synthase potentiates the neurotrophic effects of brain-derived neurotrophic factor on axotomized retinal ganglion cells in vivo. *J Neurosci* 18: 1038–1046, 1998.
56. Koh JY, Gwag BJ, Lobner D, and Choi DW. Potentiated necrosis of cultured cortical neurons by neurotrophins. *Science* 268: 573–575, 1995.
57. Kolarow R, Kuhlmann CRW, Munsch T, Zehendner C, Brigadski T, Luhmann HJ, and Lessmann V. BDNF-induced nitric oxide signals in cultured rat hippocampal neurons: time course, mechanism of generation, and effect on neurotrophin secretion. *Front Cell Neurosci* 8: 323, 2014.
58. Korkotian E. Fast confocal imaging of calcium released from stores in dendritic spines. *Eur J Neurosci* 10: 2076–2084, 1998.
59. Korkotian E and Segal M. Release of calcium from stores alters the morphology of dendritic spines in cultured hippocampal neurons. *Proc Natl Acad Sci U S A* 96: 12068–12072, 1999.
60. Korte M, Carroll P, Wolf E, Brem G, Thoenen H, and Bonhoeffer T. Hippocampal long-term potentiation is impaired in mice lacking brain-derived neurotrophic factor. *Proc Natl Acad Sci U S A* 92: 8856–8860, 1995.
61. Kovalchuk Y, Hanse E, Kafitz KW, and Konnerth A. Postsynaptic induction of BDNF-mediated long-term potentiation. *Science* 295: 1729–1734, 2002.
62. Kuczewski N, Porcher C, Ferrand N, Fiorentino H, Pellegrino C, Kolarow R, Lessmann V, Medina I, and Gaiarsa JL. Backpropagating action potentials trigger dendritic release of BDNF during spontaneous network activity. *J Neurosci* 28: 7013–7023, 2008.
63. Leite MF, Burgstahler AD, and Nathanson MH. Ca^{2+} waves require sequential activation of inositol trisphosphate receptors and ryanodine receptors in pancreatic acini. *Gastroenterology* 122: 415–427, 2002.
64. Lessmann V, Gottmann K, and Heumann R. BDNF and NT-4/5 enhance glutamatergic synaptic transmission in cultured hippocampal neurones. *Neuroreport* 6: 21–25, 1994.
65. Lessmann V and Heumann R. Modulation of unitary glutamatergic synapses by neurotrophin-4/5 or brain-derived neurotrophic factor in hippocampal microcultures: presynaptic enhancement depends on pre-established paired-pulse facilitation. *Neuroscience* 86: 399–413, 1998.
66. Levine ES, Crozier RA, Black IB, and Plummer MR. Brain-derived neurotrophic factor modulates hippocampal synaptic transmission by increasing N-methyl-D-aspartic acid receptor activity. *Proc Natl Acad Sci U S A* 95: 10235–10239, 1998.
67. Levine ES, Dreyfus CF, Black IB, and Plummer MR. Brain-derived neurotrophic factor rapidly enhances synaptic transmission in hippocampal neurons via postsynaptic tyrosine kinase receptors. *Proc Natl Acad Sci U S A* 92: 8074–8077, 1995.
68. Levine ES and Kolb JE. Brain-derived neurotrophic factor increases activity of NR2B-containing N-methyl-D-aspartate receptors in excised patches from hippocampal neurons. *J Neurosci Res* 62: 357–362, 2000.
69. Li Y, Calfa G, Inoue T, Amaral MD, and Pozzo-Miller L. Activity-dependent release of endogenous BDNF from mossy fibers evokes a TRPC3 current and Ca^{2+} elevations in CA3 pyramidal neurons. *J Neurophysiol* 103: 2846–2856, 2010.
70. Lin SY, Wu K, Levine ES, Mount HT, Suen PC, and Black IB. BDNF acutely increases tyrosine phosphorylation of the NMDA receptor subunit 2B in cortical and hippocampal postsynaptic densities. *Brain Res Mol Brain Res* 55: 20–27, 1998.
71. Lippman J and Dunaevsky A. Dendritic spine morphogenesis and plasticity. *J Neurobiol* 64: 47–57, 2005.
72. Liu X, Ramirez S, Pang PT, Puryear CB, Govindarajan A, Deisseroth K, and Tonegawa S. Optogenetic stimulation of a hippocampal engram activates fear memory recall. *Nature* 484: 381–385, 2012.
73. Lohof AM, Ip NY, and Poo MM. Potentiation of developing neuromuscular synapses by the neurotrophins NT-3 and BDNF. *Nat Lett* 363: 350–353, 1993.
74. Lu YF and Hawkins RD. Ryanodine receptors contribute to cGMP-induced late-phase LTP and CREB phosphorylation in the hippocampus. *J Neurophysiol* 88: 1270–1278, 2002.
75. Mariga A, Zavadil J, Ginsberg SD, and Chao MV. Withdrawal of BDNF from hippocampal cultures leads to

- changes in genes involved in synaptic function. *Dev Neurobiol* 75: 173–192, 2015.
76. Massaad CA and Klann E. Reactive oxygen species in the regulation of synaptic plasticity and memory. *Antioxid Redox Signal* 14: 2013–2054, 2011.
 77. Matsuzaki M, Ellis-Davies GCR, Nemoto T, Miyashita Y, Iino M, and Kasai H. Dendritic spine geometry is critical for AMPA receptor expression in hippocampal CA1 pyramidal neurons. *Nat Neurosci* 4: 1086–1092, 2001.
 78. Matsuzaki M, Honkura N, Ellis-Davies GCR, and Kasai H. Structural basis of long-term potentiation in single dendritic spines. *Nature* 429: 761–766, 2004.
 79. Mizuno M, Yamada K, He J, Nakajima A, and Nabeshima T. Involvement of BDNF receptor TrkB in spatial memory formation. *Learn Mem* 10: 108–115, 2003.
 80. Mizuno M, Yamada K, Olariu A, Nawa H, and Nabeshima T. Involvement of brain-derived neurotrophic factor in spatial memory formation and maintenance in a radial arm maze test in rats. *J Neurosci* 20: 7116–7121, 2000.
 81. Muñoz P, Humeres A, Elgueta C, Kirkwood A, Hidalgo C, and Núñez MT. Iron mediates N-Methyl-D-aspartate receptor-dependent stimulation of calcium-induced pathways and hippocampal synaptic plasticity. *J Biol Chem* 286: 13382–13392, 2011.
 82. Nägerl UV, Eberhorn N, Cambridge SB, and Bonhoeffer T. Bidirectional activity-dependent morphological plasticity in hippocampal neurons. *Neuron* 44: 759–767, 2004.
 83. Nakazawa T, Komai S, Tezuka T, Hisatsune C, Umemori H, Semba K, Mishina M, Manabe T, and Yamamoto T. Characterization of Fyn-mediated tyrosine phosphorylation sites on GluR2 (NR2B) subunit of the N-methyl-D-aspartate receptor. *J Biol Chem* 276: 693–699, 2001.
 84. Nguyen PV and Kandel ER. A macromolecular synthesis-dependent late phase of long-term potentiation requiring cAMP in the medial perforant pathway of rat hippocampal slices. *J Neurosci* 16: 3189–3198, 1996.
 85. Nguyen PV and Kandel ER. Brief theta-burst stimulation induces a transcription-dependent late phase of LTP requiring cAMP in area CA1 of the mouse hippocampus. *Learn Mem* 4: 230–243, 1997.
 86. Nimchinsky EA, Sabatini BL, and Svoboda K. Structure and function of dendritic spines. *Annu Rev Physiol* 64: 313–353, 2002.
 87. Oertner TG and Matus A. Calcium regulation of actin dynamics in dendritic spines. *Cell Calcium* 37: 477–482, 2005.
 88. Ohnuki T and Nomura Y. 1-(((5-(4-Nitrophenyl)-2furanyl)methylene)imino)-2,4-imidazolidinedione (dantrolene), an inhibitor of intracellular Ca²⁺ mobilization, impairs avoidance performance and spatial memory in mice. *Biol Pharm Bull* 19: 1038–1040, 1996.
 89. Okamoto K, Nagai T, Miyawaki A, and Hayashi Y. Rapid and persistent modulation of actin dynamics regulates postsynaptic reorganization underlying bidirectional plasticity. *Nat Neurosci* 7: 1104–1112, 2004.
 90. Oliveira AM and Bading H. Calcium signaling in cognition and aging-dependent cognitive decline. *Biofactors* 37: 168–174, 2011.
 91. Park H and Poo MM. Neurotrophin regulation of neural circuit development and function. *Nat Rev Neurosci* 14: 7–23, 2013.
 92. Paula-Lima AC, Adasme T, SanMartín C, Sebollela A, Hetz C, Carrasco MA, Ferreira ST, and Hidalgo C. Amyloid β -peptide oligomers stimulate RyR-mediated Ca²⁺ release inducing mitochondrial fragmentation in hippocampal neurons and prevent RyR-mediated dendritic spine remodeling produced by BDNF. *Antioxid Redox Signal* 14: 1209–1223, 2011.
 93. Paula-Lima AC, Adasme T, and Hidalgo C. Contribution of Ca²⁺ release channels to hippocampal synaptic plasticity and spatial memory: potential redox modulation. *Antioxid Redox Signal* 21: 892–914, 2014.
 94. Paxinos G and Watson C. *The Rat Brain in Stereotaxic Coordinates*. San Diego, CA: Academic Press, 1998, p. 34.
 95. Pfaffl MW. A new mathematical model for relative quantification in real-time RT-PCR. *Nucleic Acids Res* 29: e45, 2001.
 96. Pozzo-Miller LD, Gottschalk W, Zhang L, McDermott K, Du J, Gopalakrishnan R, Oho C, Sheng ZH, and Lu B. Impairments in high-frequency transmission, synaptic vesicle docking, and synaptic protein distribution in the hippocampus of BDNF knockout mice. *J Neurosci* 19: 4972–4983, 1999.
 97. Raymond CR, and Redman SJ. Different calcium sources are narrowly tuned to the induction of different forms of LTP. *J Neurophysiol* 88: 249–255, 2002.
 98. Rey FE, Cifuentes ME, Kiarash A, Quinn MT, and Pagano PJ. Novel competitive inhibitor of NAD(P)H oxidase assembly attenuates vascular O(2)(-) and systolic blood pressure in mice. *Circ Res* 89: 408–414, 2001.
 99. Reyes-Harde M, Potter BV, Galione A, and Stanton PK. Induction of hippocampal LTD requires nitric-oxide-stimulated PKG activity and Ca²⁺ release from cyclic ADP-ribose-sensitive stores. *J Neurophysiol* 82: 1569–1576, 1999.
 100. Richards DA, Mateos JM, Hugel S, de Paola V, Caroni P, Gähwiler BH, McKinney RA. Glutamate induces the rapid formation of spine head protrusions in hippocampal slice cultures. *Proc Natl Acad Sci U S A* 102: 6166–6171, 2005.
 101. Riquelme D, Alvarez A, Leal N, Adasme T, Espinoza I, Valdés JA, Troncoso N, Hartel S, Hidalgo J, Hidalgo C, and Carrasco MA. High-frequency field stimulation of primary neurons enhances ryanodine-receptor-mediated Ca²⁺ release and generates hydrogen peroxide, which jointly stimulate NF- κ B activity. *Antioxid Redox Signal* 14: 1245–1259, 2011.
 102. Rostas JA, Brent VA, Voss K, Errington ML, Bliss TV, and Gurd JW. Enhanced tyrosine phosphorylation of the 2B subunit of the N-methyl-D-aspartate receptor in long-term potentiation. *Proc Natl Acad Sci U S A* 93: 10452–10456, 1996.
 103. Sabatini BL, Oertner TG, and Svoboda K. The life cycle of Ca²⁺ ions in dendritic spines. *Neuron* 33: 439–452, 2002.
 104. Samdani AF, Newcamp C, Resink A, Facchinetti F, Hoffman BE, Dawson VL, and Dawson TM. Differential susceptibility to neurotoxicity mediated by neurotrophins and neuronal nitric oxide synthase. *J Neurosci* 17: 4633–4641, 1997.
 105. Segal RA and Greenberg ME. Intracellular signaling pathways activated by neurotrophic factors. *Annu Rev Neurosci* 19: 463–489, 1996.
 106. Serrano F and Klann E. Reactive oxygen species and synaptic plasticity in the aging hippocampus. *Ageing Res Rev* 3: 431–443, 2004.
 107. Sherwood NT and Lo DC. Long-term enhancement of central synaptic transmission by chronic brain-derived neurotrophic factor treatment. *J Neurosci* 19: 7025–7036, 1999.

108. Suen PC, Wu K, Levine ES, Mount HT, Xu JL, Lin SY, and Black IB. Brain-derived neurotrophic factor rapidly enhances phosphorylation of the postsynaptic N-methyl-D-aspartate receptor subunit 1. *Proc Natl Acad Sci U S A* 94: 8191–8195, 1997.
109. Sun J, Xin C, Eu JP, Stamler JS, and Meissner G. Cysteine-3635 is responsible for skeletal muscle ryanodine receptor modulation by NO. *Proc Natl Acad Sci U S A* 98: 11158–11162, 2001.
110. Tanaka J, Horiike Y, Matsuzaki M, Miyazaki T, Ellis-Davies GC, and Kasai H. Protein synthesis and neurotrophin-dependent structural plasticity of single dendritic spines. *Science* 319: 1683–1687, 2008.
111. Tejada-Simon MV, Serrano F, Villasana LE, Kanterewicz BI, Wu GY, Quinn MT, Klann E. Synaptic localization of a functional NADPH oxidase in the mouse hippocampus. *Mol Cell Neurosci* 29: 97–106, 2005.
112. Tsay D and Yuste R. On the electrical function of dendritic spines. *Trends Neurosci* 27: 77–83, 2004.
113. Tyler WJ, Alonso M, Bramham CR, and Pozzo-Miller LD. From acquisition to consolidation: on the role of brain-derived neurotrophic factor signaling in hippocampal-dependent learning. *Learn Mem* 9: 224–237, 2002.
114. Vlachos A, Korkotian E, Schonfeld E, Copanaki E, Deller T, and Segal M. Synaptopodin regulates plasticity of dendritic spines in hippocampal neurons. *J Neurosci* 29: 1017–1033, 2009.
115. Wilson C, Muñoz-Palma E, Henríquez DR, Palmisano I, Núñez MT, Di Giovanni S, and González-Billault C. A feed-forward mechanism involving the NOX complex and RyR-mediated Ca²⁺ release during axonal specification. *J Neurosci* 36: 11107–11119, 2016.
116. Xu Z, Ji X, and Boysen PG. Exogenous nitric oxide generates ROS and induces cardioprotection: involvement of PKG, mitochondrial KATP channels, and ERK. *Am J Physiol Heart Circ Physiol* 286: H1433–H1440, 2004.
117. Yan Y, Chao-Liang W, Wan-rui Z, He-ping C, and Jie L. Cross-talk between calcium and reactive oxygen species signaling. *Acta Pharmacol Sin* 27: 821–826, 2006.
118. Zagrebelsky M and Korte M. Form follows function: BDNF and its involvement in sculpting the function and structure of synapses. *Neuropharmacology* 76: 628–638, 2014.
119. Zhao W, Meiri N, Xu H, Cavallaro S, Quattrone A, Zhang L, and Alkon DL. Spatial learning induced changes in expression of the ryanodine type II receptor in the rat hippocampus. *FASEB J* 14: 290–300, 2000.
120. Zhou Q, Homma KJ, and Poo MM. Shrinkage of dendritic spines associated with long-term depression of hippocampal synapses. *Neuron* 44: 749–757, 2004.
121. Zima AV and Blatter LA. Redox regulation of cardiac calcium channels and transporters. *Cardiovasc Res* 71: 310–321, 2006.
122. Ziviani E, Lippi G, Bano D, Munarriz E, Guiducci S, Zoli M, Young KW, and Nicotera P. Ryanodine receptor-2 upregulation and nicotine-mediated plasticity. *EMBO J* 30: 194–204, 2011.

Address correspondence to:

Dr. Tatiana Adasme
 Centro Integrativo de Biología y Química Aplicada
 Universidad Bernardo O'Higgins
 General Gana 1702
 Santiago 8370854
 Chile

E-mail: tatiana.adasme@ubo.cl

Date of first submission to ARS Central, July 11, 2017; date of final revised submission, January 17, 2018; date of acceptance, January 20, 2018.

Abbreviations Used

4-CMC	= 4-chloro-m-cresol
A β Os	= amyloid β -peptide oligomers
ANOVA	= analysis of variance
BDNF	= brain-derived neurotrophic factor
cDNA	= complementary DNA
CICR	= Ca ²⁺ -induced Ca ²⁺ release
CREB	= cAMP response element-binding
Ct	= cycle threshold
DIV	= days <i>in vitro</i>
GFP	= green fluorescent protein
gpscr	= Gp91 ds-tat inactive scrambled peptide
H ₂ O ₂	= hydrogen peroxide
IP ₃	= inositol 1,4,5-trisphosphate
IP ₃ R	= IP ₃ receptors
LTP	= long-term potentiation
mRNA	= messenger RNA
NAC	= N-acetylcysteine
NMDA	= N-methyl-D-aspartate
NOS	= nitric oxide synthase
NOX2	= NADPH oxidase type-2
ODN-RyR2	= RyR2-directed antisense oligodeoxynucleotides
ODN-Scr	= scrambled sequence of RyR2-directed antisense oligodeoxynucleotides
PBS	= phosphate-buffered saline
PKG	= protein kinase G
PLC γ	= phospholipase C γ
qPCR	= quantitative polymerase chain reaction
RFP	= red fluorescent protein
RNS	= reactive nitrogen species
ROS	= reactive oxygen species
RyR	= ryanodine receptor
RyR2	= ryanodine receptor type-2
SE	= standard error
shRNA	= short hairpin RNA
shRyR2	= shRNA against RyR2
shScr	= shRNA against the scrambled RyR2 sequence